FORSCHUNGSZENTRUM JÜLICH GmbH

KFA

Institut für Werkstoffe der Energietechnik

Structural Investigations of Carburized Alloy 800H

A. Czyrska-Filemonowicz P.J. Ennis F. Ciura
K. Spiradek

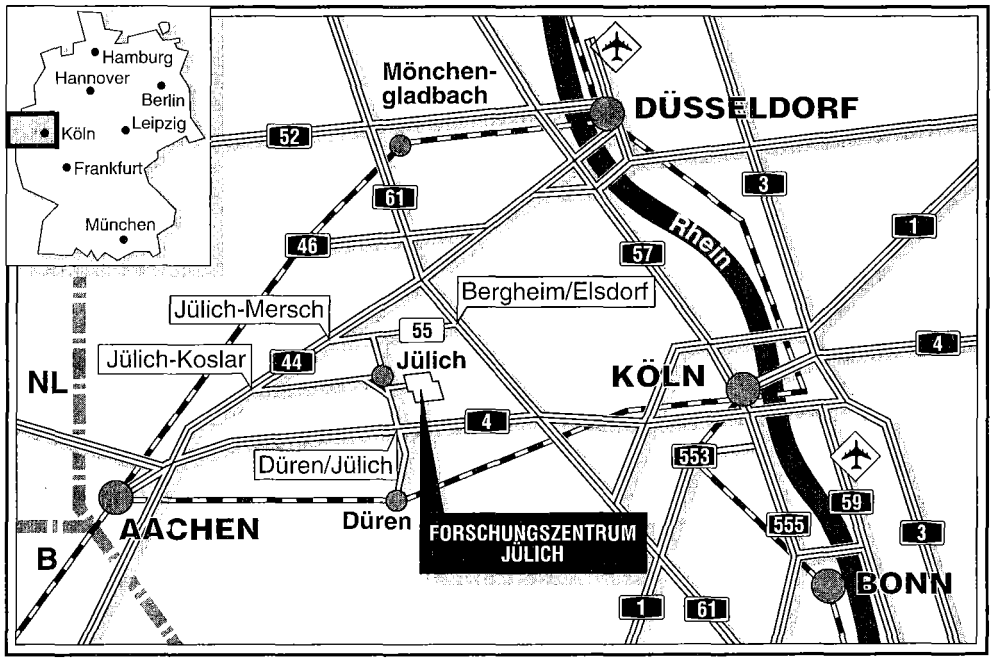

Berichte des Forschungszentrums Jülich ; 3138
ISSN 0944-2952
Institut für Werkstoffe der Energietechnik Jül-3138

Zu beziehen durch: Forschungszentrum Jülich GmbH · Zentralbibliothek
D-52425 Jülich · Bundesrepublik Deutschland
Telefon: 02461/61-6102 · Telefax: 02461/61-6103 · Telex: 833556-70 kfa d

Structural Investigations of Carburized Alloy 800H

A. Czyrska-Filemonowicz[1] P.J. Ennis[2] F. Ciura[3]
K. Spiradek[4]

[1] Guest Scientist Forschungszentrum Jülich GmbH, D-52425 Jülich, Germany
on leave from the University of Mining and Metallurgy, Kraków, Poland
[2] Forschungszentrum Jülich GmbH, D-52425 Jülich, Germany
[3] University of Mining and Metallurgy, Kraków, Poland
[4] Österreichisches Forschungszentrum, Seibersdorf, Austria

Structural investigations of carburized Alloy 800H

by

A. Czyrska-Filemonowicz
P.J. Ennis
F. Ciura
K. Spiradek

Abstract

The effect of carburization on the impact strength and microstructure of the commercial Alloy 800H (Fe-32Ni-20Cr) has been investigated in the temperature range 20 - 800°C. The properties and microstructure of test pieces carburized at 850°C for up to 500 h in an argon - 10 volume % methane atmosphere and of specimens aged at 850°C in an inert atmosphere for the same times were compared. Microstructural investigations by optical metallography, and transmission and scanning electron microscopy showed the details of the microstructure after ageing and carburization at 850°C.

The results showed that ageing at 850°C reduced the impact strength in the range 20 - 800°C. With increasing degree of carburization, the impact strength was progressively reduced to around 50 J at a bulk carbon content of 0.6 wt %.

Effects of carburization on the microstructure and mechanical properties of Alloy 800H are discussed.

Untersuchungen der Mikrostruktur von aufgekohltem Alloy 800H

von

A. Czyrska-Filemonowicz
P.J. Ennis
F. Ciura
K. Spiradek

Kurzfassung

Es wurde der Einfluß einer Aufkohlung auf die Kerbschlagarbeit und das Gefüge der kommerziellen Legierung Alloy 800H (Fe-32Ni-20Cr) im Temperaturbereich 20 bis 800°C untersucht. Die Eigenschaften und die Struktur von aufgekohlten Proben (500 h bei 850°C in Ar-10 Vol. % CH4) wurden mit den Eigenschaften und der Struktur von ausgelagerten Proben als Referenz (500 h bei 850°C in Argon) verglichen.

Die Gefügeänderungen der Proben wurden mittels Transmissions- und Raster-Elektronenmikroskopie sowie Metallographie bestimmt.

Die Ergebnisse zeigen, daß schon die Auslagerung bei 850°C die Kerbschlagzähigkeit im Temperaturbereich 20 bis 800°C vermindert. Mit zunehmender Aufkohlung wird die Kerbschlagarbeit noch weiter reduziert. Bei einem integralen Kohlenstoffgehalt bis zu 0,6 Mass.-% verbleibt im Bereich 20 bis 800°C ein Restwert von 50 J.

Der Einfluß der Aufkohlung auf die mechanischen Eigenschaften der Legierung Alloy 800H wird anhand der Information über die Gefügeentwicklung interpretiert.

CONTENTS

1. INTRODUCTION

The good corrosion and oxidation resistance, high strength and excellent fabricability of Alloy 800 (Fe 32wt%Ni20wt%Cr) coupled with its relatively low cost have led to extensive use of the alloy. Typical applications include furnace and heat treatment equipment, and components for petrochemical and power generation plants including nuclear stations. Alloy 800 steam generator tubes are used, for example, in the German PWRs (operating temperature ca 300 °C), in heavy water CANDU reactors and are to be used in fast breeder reactors; the mechanical properties at temperatures up to 550 °C and excellent resistance to pitting and stress corrosion in aqueous environments are the main reasons for selecting the alloy. Because of the wide range of applications for the alloy, the collection of data and the establishment of design codes and specifications have been encouraged. The technical and scientific interest in Alloy 800 is well illustrated by the fact that three international conferences devoted exclusively to discussion of the alloy and its properties have been held /1, 2, 3/.

For high temperature applications where the design is made on the basis of time-dependent properties, a high carbon modification of Alloy 800, designated 800 H, is recommended. The higher carbon content (0,05 - 0,1 wt%) and the heat treatment (solution annealing at around 1150 °C) specified to promote a coarse-grained microstructure (grain size > ASTM 5) allow somewhat higher creep rupture strengths to be achieved. Alloy 800 H is already included in high temperature design rules for nuclear components at temperatures up to 760 °C /4/ and has been used for the steam generator tubes in the high temperature power reactor (HTR) Fort St. Vrain, USA and THTR, Schmeehausen, FRG; maximum operating temperatures are around 750 °C.

Although unsuitable for the components operating at the highest temperatures of 950 °C in a process heat HTR system, for which nickel-base alloys with their higher creep rupture strength are required, Alloy 800 H could be used for many components which operate at temperatures up to 850 °C.

In the present investigation, the effects of carburization, which can occur under some service conditions, for example in low oxygen potential impure helium containing traces of methane, carbon monoxide and water, the anticipated composition of HTR primary circuit coolant, on the impact properties and the microstructure of Alloy 800 H in the temperature range 20 - 800 °C have been determined. The changes in

impact strength have been correlated with the results of microstructural investigations.

2. THE STRUCTURE OF ALLOYS 800 AND 800H

The high nickel content of this iron-base alloy ensures a fully austenitic matrix structure. The presence of minor, but important, amounts of carbon, titanium and aluminium, which originate largely from the use of superalloy scrap in the melting charge, causes precipitates to form in the matrix during solidification, heat treatment and service exposure. The most important precipitates are the carbides $M_{23}C_6$ (chromium-rich) and TiC. Other precipitates which have been observed are γ' (Ni_3(Al, Ti)) and G phase ($Ni_{16}Ti_6Si_7$).

2.1 Carbide precipitation

The type of carbide precipitated during thermal ageing or service exposure is dependent on

- the chemical composition of the alloy within the specification range, more precisely on the ratio of titanium to carbon and nitrogen contents;

- the ageing or service conditions: time, temperature and environment.

Orr /5/ summarized the precipitation reactions occurring in Alloy 800 H as shown in Fig. 1.

Degischer et al /6, 7/ have shown schematic diagrams of carbide precipitation in Alloy 800 and Alloy 800 H (Fig. 2, 3) , which correspond well with other the experimental results published in the literature. The affinity of titanium for carbon is stronger than that of chromium and therefore under equilibrium conditions, TiC will be present rather than $M_{23}C_6$ and the concentration of carbon in solution at high temperatures will be controlled by titanium content. Although much less stable than TiC, $M_{23}C_6$ forms preferentially because of the more favourable kinetics.

As shown in precipitation diagrams the kinetics of precipitation of $M_{23}C_6$ and TiC in Alloy 800 H appear to be similar at temperatures above about 800 °C and both phases may occur in the same specimen. At temperatures of around 600 °C, the chromium-rich $M_{23}C_6$ is the predominant phase.

Microstructural investigations of Alloy 800 H aged at higher temperatures /5 - 25/ showed that intragranular $M_{23}C_6$ and TiC precipitate on dislocations. Therefore cold-working promotes the formation of intragranular precipitates by providing a higher dislocation density and hence an increase in nucleation sites for the carbides.

Grain boundary $M_{23}C_6$ carbides are frequently observed and such precipitates retain a crystallographic orientation to one grain and grow into the adjacent grain. Lamellae of $M_{23}C_6$ precipitate on non-coherent twin boundaries grow into the grain parallel to the twin plane. $M_{23}C_6$ precipitates on coherent twin boundaries grow as plates along the twinning plane.

The formation of finely dispersed, intragranular carbides leads to a significant hardening, which starts to diminish at longer ageing times and higher ageing temperatures as the precipitates begin to coarsen. Grain boundary carbides are more important in technical applications of the alloy and generally lead to a decrease in ductility and impact strength. In the creep regime, however, the grain boundary carbides make a significant contribution to the creep and rupture strength /26 - 30/.

Primary precipitates, generally large (2 - 5 µm) and angular in form, observed in Alloy 800 are titanium-rich carbides (TiC), carbonitrides (Ti(C, N)), or nitrides (TiN). These particles form from the melt and are not influenced substantially by subsequent heat treatments.

2.2 Intermetallic compound precipitation

The precipitation of γ' / 5, 10-14 /, which forms homogeneously in the matrix, can be observed in Alloy 800 H heats containing combined aluminium and titanium contents above 0.6 wt % after ageing at 550 - 750 °C, and was found to form rapidly at about 600-650 °C. At higher temperatures, the precipitate particles overage and become less effective dislocation barriers. No γ' has been observed after exposure at 800 °C. This is an indication of the solubility temperature of γ' /5/.

Precipitation of γ' phase is associated with an increase in strength and a small decrease in ductility in room temperature tensile tests. The spherical shape of the particles indicates a low lattice parameter mismatch between the precipitate and the matrix. The size of the coherent γ' particles has an important effect on the creep and fatigue resistance, where intragranular particles interact strongly with mobile dislocations. The relatively large γ' particles formed in Alloy 800 aged at 600 °C

(diameter > 200 nm) are by-passed according to the Orowan mechanism. Very fine γ' particles (diameter less than 25 nm) formed after ageing at 550 °C may be cut and sheared by dislocations /22 - 25/.

A deleterious effect of γ' precipitation on creep-rupture ductility has been reported in tests at 550 - 650 °C /17, 18/. The low ductility be avoided by:

- limiting (Ti+Al) to maximum of 0.56 % in low carbon alloy (C < 0.05 %)

- limiting (Ti+Al) to maximum of 0.65 % in higher carbon alloy (C > 0.05 %).

The amount of silicon in the alloy is important for the precipitation of γ'; reducing the silicon content from 0.6 % to 0.3 % causes an increase in the matrix solubility for (Ti+Al) from 0.6 % to 0.8 %, thereby reducing or even avoiding γ' precipitation.

Precipitation of G phase, $Ni_{16}Ti_6Si_7$, has been observed after long ageing times at different temperatures /5, 8 - 11/. Globular particles are formed in the vicinity of grain boundaries and lenticular precipitates grow along the grain boundaries. The morphology of G phase is similar to $M_{23}C_6$ carbide; G phase has also A1 crystal structure and a similar lattice parameter to $M_{23}C_6$. Thus, the analysis of chemical composition (e.g. by energy dispersive spectroscopy, EDS) is needed to distinguish G phase from $M_{23}C_6$ carbide.

Finally, it should be mentioned that σ phase (FeCr) has been observed in some heats of Alloy 800 after long-time ageing (e.g. 30000 h) at 600 and 650 °C /5, 10/. This phase is generally regarded as undesirable, but in Alloy 800 the amount, if present, is too small to have any significant effect on the mechanical behaviour. Some authors also observed an unknown phase, designated (appropriately) 'x', which was neither σ phase nor G phase /5, 11/.

3. EFFECTS OF CARBURIZATION ON MICROSTRUCTURE AND MECHANICAL PROPERTIES OF ALLOY 800H

Carbide formation due to thermal ageing of the supersaturated austenite can be enhanced if diffusion of carbon from the atmosphere into the alloy occurs during high temperature exposure. Carburization is often encountered in petrochemical plant (e.g methane reformers) where the alloy is in contact with gases.

In heat exchangers of nuclear heat systems (He/He intermediate heat exchanger or He-heated reformer tubes), carburization may occur due to the presence of impurities such as CO and CH_4 in the primary coolant helium. In this case, carburization not only depends on the impurity level in helium, but also on factors which influence the kinetics of the gas-metal reactions, such as gas flow rate and surface condition of the specimens. For example, in a relatively high oxygen potential atmosphere (water pressure > 1 µbar) carburization is retarded by the surface oxide film, while in low oxygen potential atmospheres (water pressure < 0.2 µbar) the carburization is controlled by the diffusion of carbon in the alloy /48 - 50/.

In addition to the enhancement of the carbides $M_{23}C_6$ and TiC which form due to thermal ageing by carburization, it is also possible for new carbide phases to appear as the carbon content increases. Grabke et al /30, 31/ investigated carburized Alloy 800H at three different stages:

(a) at low carbon activity only $M_{23}C_6$, precipitated at grain boundaries, was found.

b) for longer carburization periods and higher carbon activity environments, two carbides M_7C_3 and $M_{23}C_6$ precipitated.

(c) at very high carburization levels, with carbon contents of more than 1 wt%, only M_7C_3 carbides were detected.

Schulten et al /50/ studied the carburization of FeNiCr alloys and developed a model describing the carburization kinetics which could be used to predict the depth of carburization.

The tensile properties of carburized material tested at room temperature were determined and very low ductility was observed. Ennis et al /32, 33/ found that carburization of Alloy 800H in the range 850 - 950 °C led to progressive loss of room temperature ductility as the bulk carbon content increased. The carburized Alloy 800H with bulk carbon contents above about 0.4 wt% showed practically no room temperature ductility in tensile tests.

A more recent investigation of the influence of carburization on the tensile properties of Alloy 800H in the range 20 - 950 °C /34 - 36/ has been carried out. It was shown

that the low ductility range in tensile testing extended up to around 800 °C. At test temperatures above 800 °C, the ductility of even the heavily carburized material was similar to that of solution treated material. The low ductility was associated with fracture within the carbides at the grain boundaries. In the high ductility range (> 800 °C), failure occurred by separation of matrix and the carbide particles which themselves did not fracture.

In high temperature applications, the design is based largely on the time-dependent deformation behaviour (creep rupture properties) of alloys. The effect of ageing and carburization on the creep rupture properties of Alloy 800H has been investigated by several authors /27 - 29, 36 - 42/. It is of interest to note that creep rupture strength can be enhanced by carburization and indeed, if the grain boundary carbides are removed completely by, for example, decarburization, there is a severe loss of creep strength /29/.

4. EXPERIMENTAL

Details of the Alloy 800 H heat investigated are summarized in Table 1. Impact test pieces 10 x 10 mm (ISO V-notch standard specimens) were machined from the hot rolled, solution treated (1150 °C/0.5 h/w.q.) bar. The notch was machined before the carburizing treatment so that the notch root region was also carburized.

Specimens were given the following treatments:

a) ageing at 850 °C for 100, 250 and 500 h;
b) carburizing at 850 °C for 100, 250 and 500 h;
c) carburizing followed by a heat treatment of 500 h at 900 °C in argon.

Specimens were carburized by exposure in a gas mixture consisting of argon with 10 volume % methane, and the level of carburization was controlled by the time of exposure (100 to 500 h). This carburizing gas was chosen to produce rapid, heavy carburization of the test pieces which could be achieved only after several thousand hours exposure in a dry, simulated HTR helium atmosphere containing impurity gases in the mbar range.

Following carburization, some specimens were heat treated for a further 500 h in argon to allow diffusion of the carbon introduced during the carburization exposure to greater depths, producing a less steep carbon concentration gradient. The impact tests were carried out using a Charpy impact machine. For the elevated temperature tests, the specimens were heated for 20 minutes in a resistance-heated muffle

furnace and then quickly transferred to the impact test machine. Preliminary tests showed that at the highest test temperature (800 °C) the specimens required a 20 minute heating period at 830 °C to ensure that at the moment of impact of the pendulum the correct test temperature was attained.

For each test condition (specimen heat treatment and test temperature) three tests were carried out. After testing, one specimen from each set of three specimens was examined metallographically and the average bulk carbon content determined using a LECO carbon analyzer. From the metallographic examination, the depth of the zone containing continuous grain boundary carbide precipitates was determined.

The microstructure was investigated by optical microscopy, by scanning electron microscopy (SEM) and by transmission electron microscopy (TEM).
The samples for metallographic investigations were prepared by polishing and etching in one of the two chemical solutions. The first solution consisted of 10 ml HNO_3, 100 ml HCl, 100 ml distilled H_2O and 3 drops of Vogel`s reagent. This solution was heated to 55 - 60 °C and was used to reveal the carbides in contrast to the matrix. The second etchant consisted of 100ml $H_2O$, 1 g sodium hydroxide and 4 g potassium permanganate (Groesbeck`s reagent); this etchant was used to show the microstructures of the carburized specimens.

Fracture surfaces of the impact broken specimens (as listed in Table II) was examined by SEM equipped with an energy dispersive X-ray analyser (EDX). The specimens were prepared by the same techniques as for metallographic investigations.

Specimens which had been impact tested at room temperature were selected for microstructural investigations using TEM (specimens listed in Table III). TEM studies were performed using thin foils and extraction double-replica techniques.

Thin foils were prepared from the discs of 3 mm diameter by conventional thinning in a solution of 5 % perchloric acid in ethanol (temperature: -15 °C, voltage ca. 50 V) or in a solution of 10 % perchloric acid in glacial acetic acid (temperature: +15 °C, voltage ca 30 V) using a "Tenupol" twin-jet polishing apparatus.

Extraction double-replicas /47/ were used to study morphology of particles and to identify the precipitates.

Double-replicas were prepared as follows:

a) Preparation of thin metal foil (thickness < 0.1 mm) by mechanical thinning or by electropolishing and slight etching to reveal the precipitates.

b) Simultaneous evaporation of carbon and platinum film onto both sides of the plate and scratching the film into small squares.

c) Removing the matrix in a 10 % solution of bromine in ethanol. The solution dissolves the matrix but does not attack carbides, nitrides oxides, or sulphides which may be present. When the squares of replica float free, it is necessary to clean them.

d) Chemical cleaning of the replicas: 10% solution of hydrochloric acid in ethanol (30 min) followed by cleaning in the mixture of ethanol and distilled water (1:1) and by water.

e) Picking up the replicas on support grid and drying.

The investigations were performed using the Philips 400 and JEM 100C electron microscopes. The particles were identified using selected area diffraction patterns (SAD), an energy dispersive X-ray analyser (EDX) and by means of X-ray phase analysis of electrolytic extractions.

5. RESULTS AND DISCUSSION

The impact test results and the bulk carbon contents of carburized specimens are summarized in Table IV. In some instances, one of the three impact tests carried out with material in the same condition and the same temperatures was significantly higher or lower than the other two tests, and these values were not used in establishing the average impact strength (values in parenthesis in Table IV).

5.1 Carburization kinetics

Fig. 4 shows the increase in bulk carbon content and depth of the carburized zone as a function of exposure time at 850 °C in argon with 10 % methane. The results indicate a linear carburization rate which is consistent with the high carbon activity and low oxidizing potential of the gas mixture used. The depth of the carburized zone (in which continuous grain boundary precipitates were present) was measured for each of the carburized specimens from the micrographs.

5.2 Impact strength

Fig. 5 shows the variation of impact strength with temperature for Alloy 800H in the following conditions:

- solution treated at 1150 °C.
- aged for 100, 250 and 500 h at 850 °C in argon - 10% methane.
- carburized as above followed by heat treatment for 500h at 900 °C in argon.

The specimens tested in the solution treated condition showed a slight fall in impact strength as the temperature increased from 20 to 600 °C. Ageing for 100 to 500 h at 850 °C significantly reduced the impact strength at room temperature. However, at 400 °C the impact strengths of the aged and of the solution treated specimens were similar, and at 600 and 800 °C, the aged specimens showed slightly lower impact strengths than the solution treated specimens. The curve for the aged material indicated a minimum of ca 160 J at 600 °C.

Carburizing to produce a bulk carbon content of 0.10 wt%, which is still within the specified carbon range for Alloy 800H, hardly affected the impact strength; the curve was similar to that of the aged material. Heat treatment of the 0.10 wt% carbon specimens for 500h at 900 °C, however, reduced the impact strength slightly. As for the material aged at 850 °C, both curves for the 0.10 % carbon material showed a minimum impact strength at 600 °C.

Increasing the bulk carbon content to 0.6 % led to a further decrease in impact strength, which did not change significantly as the test temperature increased. The specimens heat treated after the carburization exposure showed again lower impact strength than carburized specimens. At a bulk carbon content of 0.6%, impact strengths were between 40 and 60 J.

5.3 Structural analysis

Typical microstructures revealed by optical microscopy and TEM are presented in Figs. 6 - 28. The micrographs obtained from optical microscopy allow description of the structure only in general terms, since in most cases the precipitates were too fine to be resolved by optical microscopy. A detailed evaluation is based on the results of TEM.

a) Microstructure of as-received material

Figs. 6a-c show the microstructure of as-received material; solution treated at 1150 °C /0.5 h/ water quenched. The structure of solution treated Alloy 800H consisted of austenitic matrix with primary particles, which after extraction were identified as titanium nitrides TiN or titanium carbonitrides Ti(C, N) (Fig. 6b). A small amount of $M_{23}C_6$ formed during cooling was also visible (Fig. 6c). Some non-metallic inclusions (e.g. α-SiO_2) were also detected by means of X-ray phase analysis.

b) Microstructure of the alloy aged at 850 °C (specimens A1, A2)

Figs. 7 - 16 show the microstructure of the alloy aged at 850 °C for 100 h (specimen A1) and for 500 h (specimen A2) in argon followed by impact testing at room temperature.

During isothermal ageing at 850 °C chromium-rich $M_{23}C_6$ carbides precipitated in the austenite matrix. Metallographic investigations revealed a fairly continuous layer of grain boundary carbides as well as the carbides growing parallel to twin boundaries (Figs.7, 11). The grains contain some fine particles and larger precipitates of primary titanium compounds.

Structural analysis made by TEM confirmed that $M_{23}C_6$ carbides were precipitated inter- and intragranularly. The morphology of these carbides depended on the site of nucleation and on ageing time. The grain boundary carbides have grown at well separated intervals along the boundary or they formed a continuous layer along the boundary (Fig. 10a). The grain boundary carbides grow with a parallel orientation to one of the adjacent grains, which was established by electron diffraction (SAD). SAD patterns shown in Fig. 10b, reveal parallel crystallographic orientation of the matrix lattice (intense spots) and $M_{23}C_6$ lattice (faint spots). $M_{23}C_6$ was observed also at the triple points (Fig. 12).

The twin boundary carbides were precipitated on non-coherent twin boundaries as a lamellae of carbides which grow into the grain in <110> g directions parallel to the twinning plane (Figs. 9, 13) and on coherent twin boundaries as plates aligned with the twin plane (Fig.14).

Carbides precipitated intragranularly were smaller in comparison to those formed intergranularly (Fig. 8). The morphology of these carbides was investigated using extraction double-replicas. $M_{23}C_6$ carbides extracted from the matrix are shown in

Fig. 15. In the specimen aged for 500 h (specimen A2) very fine (up to ca 15 nm in diameter) secondary titanium carbides were observed as shown in Fig. 16.

In both specimens some $M_{23}C_6$ carbides precipitated on primary titanium carbonitrides were found within the grains (Fig. 25). Similar "double-phase" precipitates have already been observed in Alloy 800 /8, 21/.

c) Microstructure of alloy carburized at 850 °C (specimens B1, B2)

Figs. 17 - 26 show the microstructure of the alloy carburized at 850 °C in argon-10 vol. % methane for 100 h (specimen B1) and for 500 h (specimen B2) followed by impact test at room temperature.

The microstructure investigated by optical microscopy allows two zone in the cross-section of the specimen to be distinguished. The outer zone contains continuous grain boundary carbide layers and significantly greater volume fraction of intragranular carbides. In this zone precipitation is more intense and there is the possibility of M_7C_3 carbide formation (Figs. 17, 29).

Structural analysis by TEM has been performed for the outer and inner zone separately. The structure of outer, carburized zone consisted of large amount of intragranular $M_{23}C_6$ carbides as well as of intergranular carbides forming a continuous layer along the boundaries (Fig. 18). Large, chromium-rich M_7C_3 carbides were observed in this zone (Figs. 19, 20). The morphology of these carbides extracted on the replica is shown in Fig. 19. These carbides often contain planar defects (stacking faults or microtwins). An electron diffraction (SAD) pattern taken from individual carbide particle is shown in Fig. 20c. The presence of streaks in SAD pattern lying in directions in the basal plane of pseudohexagonal crystal structure of Cr_7C_3 is interpreted in terms of stacking faults on and perpendicular to the basal planes {0001} and {1120}. Beach and Warrington /43/ have used this characteristic streaking as a means of distinguishing this carbide from others. Planar defects in the crystalline lattice of M_7C_3 carbides were observed in various alloys /43 - 46/.

The precipitate in the inner zone consisted mainly of $M_{23}C_6$ carbides, which precipitated on grain boundaries and created fairly continuous carbide layers along the boundary (Figs. 22, 24). One side of the particle interface follows the grain boundary, while the other side has a serrated appearance indicating a preferred orientation with the adjacent grain. The widely spaced interfacial dislocations indicate

a low lattice mismatch between $M_{23}C_6$ carbide and the matrix. This was confirmed by electron diffraction which showed a parallel orientation between the cubic lattices of matrix and precipitate on this side of the boundary. $M_{23}C_6$ carbides precipitated also at the twin boundaries (Fig. 23) as well as within the grains. Precipitates of $M_{23}C_6$ carbides around primary titanium carbonitrides were also observed (Fig. 25). The morphology of the intragranular $M_{23}C_6$ carbides extracted on replicas is shown in Fig. 26. M_7C_3 carbides were not observed in the inner layer of both specimens investigated.

d) Microstructure of alloy heated at 900 °C after carburization treatment (specimen C).

Fig. 27 shows the microstructure of the Alloy 800 H heat treated for 500 h at 900 °C following carburization for 500 h at 850 °C and impact testing at room temperature. The grain boundary carbides have become thicker and the precipitation-free zone near the grain boundaries has increased in width.

The morphology of $M_{23}C_6$ carbides was investigated using extraction replicas that showed plate-like and cuboidal shapes which suggested that coarsening of precipitates has occurred (Fig. 28a). Secondary titanium carbides TiC were precipitated within the grains (Fig. 28b) and were much finer (ca 15 nm in diameter) in comparison with the size of chromium carbides (up to 1 μm in diameter). As usual, primary titanium carbonitrides were also observed.

The fracture facets of the broken specimens (as listed in Table II) were examined by SEM. Figs. 29a-d show the fracture facets of the specimen A2 (aged at 850 °C for 500 h) impact tested at RT, 400, 600 and 800 °C. The fracture of Alloy 800 H was transgranular, ductile fracture for all impact testing temperatures.

Figs. 30 and 31 show the fracture facets of the broken specimen B2 (carburized at 850 °C for 500 h) impact tested at RT and 800 °C. Fig. 32 shows the fracture of specimen heated at 900 °C/500 h after carburization and impact tested at 800 °C. In all the specimens investigated, the carburized zone always fractured along the grain boundary carbides and exhibited intergranular fracture, whereas the non-carburized core exhibited a ductile fracture behaviour (transgranular fracture).

5.4 Structure-property relationship

Notched specimens carburized at 850 °C up to 500 h were impact tested in the temperature range 20 - 800 °C. The results are shown in Fig. 5 together with the impact strengths of specimens heat-treated in argon for times similar to those of the carburization exposure. The results showed that ageing at 850 °C reduced the impact strength at 20 - 800 °C. With increasing degree of carburization, the impact strength was progressively reduced to around 70 J/cm^2 at a bulk carbon content of 0.5 wt %. Heat treatment after carburization caused a further decrease in impact strength as the depth of carbon penetration increased. Metallographic examination showed that at the highest carburization level, continuous grain boundary carbide to depths of 3 - 4 mm from surface had formed.

Optical metallography investigations of Alloy 800 H carburized at 850 °C for 100 and 500 h revealed two zones in the cross-section of the specimens:

- carburized zone which contains M_7C_3 and $M_{23}C_6$ carbides;

- inner zone (non-carburized core) in which the structure was similar to the structure formed by ageing in argon.

The formation of two layers of Cr-rich carbides (M_7C_3 and $M_{23}C_6$) in the heavily carburized Alloy 800 H has been reported in literature /26, 30, 31, 39/.

TEM investigations have been performed for each zone separately. In the outer, carburized layer, large chromium-rich M_7C_3 carbides with characteristic planar defects were observed. Large amounts of intragranular $M_{23}C_6$ carbides as well as intergranular $M_{23}C_6$ which form a continuous layer along the grain boundaries were present. The structure of non-carburized core was similar to the aged structure and consisted mainly of $M_{23}C_6$ precipitated within the grain. Secondary TiC precipitates were also observed within the grains and were much finer in comparison with the $M_{23}C_6$ carbides. As usual, primary Ti(C,N) were also observed.

SEM investigations of fracture facets of the broken impact test pieces were performed. The carburized zone always fracture along the grain boundaries and exhibited intergranular fracture, whereas the inner zone revealed a ductile, transgranular fracture behaviour.

6. CONCLUSIONS

6.1 Ageing at 850 °C for up to 500 h produced grain boundary precipitation of $M_{23}C_6$, which reduced the notched impact strength at temperatures in the range 20 - 800 °C.

6.2 The structure of Alloy 800 H aged at 850 °C consisted of austenite matrix with precipitated carbides, mainly chromium-rich $M_{23}C_6$.

$M_{23}C_6$ carbides precipitated on grain boundaries retained crystallographic orientation to one of the austenite grains and grew into the adjacent grain. Lamellae of $M_{23}C_6$ carbides precipitated on non-coherent twin boundaries grew into the grain parallel to the twinning plane. $M_{23}C_6$ carbides precipitated on coherent twin boundaries grew as plates along the twinning plane.

Within the grains chromium carbides $M_{23}C_6$ were precipitated on dislocations and occasionally on the interfaces of primary Ti(C,N). Fine (up to 15 nm) secondary TiC as well as large (2 - 5 μm) primary Ti(C,N) were also observed within the grains.

6.3 Carburization significantly reduced the impact strength, the degree of embrittlement depending on the depth of the carburized zone (exposure time).

6.4 In the cross-section of the alloy carburized at 850 °C two zones could be distinguished; a carburized zone with enhanced precipitation of M_7C_3 as well as $M_{23}C_6$ and a non-carburized core with $M_{23}C_6$. The carburized zone always fractured along the grain boundaries and exhibited intergranular fracture whereas the inner zone revealed a ductile transgranular fracture behaviour.

ACKNOWLEDGEMENT

One of the authors (A. C-F.) would like to thank Professor H Nickel and all colleagues in the Institute for Materials in Energy Systems 1, Research Centre Jülich, for their kind hospitality during her stay at KFA.

REFERENCES

/1/ "Status Review of Alloy 800", Proceedings of BNES Conference, Reading University, September 25-26, (1974), ed. S.F. Pugh, AERE Harwell 1974

/2/ "Alloy 800", Proceedings of the Petten International Conference, March 14-16 (1987), The Netherlands, ed. W. Betteridge et al., North Holland Publishing Company, Amsterdam 1980

/3/ "High-temperature Metallic Materials for Gas-cooled Reactors", Proc. IAEA Specialists' Meeting, Vienna, June 4-6 (1981), ed. IAEA Vienna 1982

/4/ H. Nickel, F. Schubert, H. Schuster: Nuclear Eng. and Design 94 (1986) 337

/5/ J. Orr, in ref. 2, p. 25

/6/ H. P. Degischer, H. Aigner: Proceedings of the International Colloquium on Stainless Steel, Saint Etienne (1982) 16

/7/ H. P. Degischer, H. Aigner, H. Lahodny, K. Spiradek: Conference "High Temperature Alloys - Their Exploitable Potential", JRC Petten, NL, 15-17th Oct 1985, Publ by Elsevier Applied Science London, New York, EUR 11365, ed J.B.Marriot, M.Merz, J.Nihoul, J.O.Ward, 1987, pp 465-474

/8/ H. Aigner, O. Demel, H.P. Degischer: Zeitschrift für Werkstofftechnik 14 (1983) 24

/9/ A. Czyrska-Filemonowicz, K. Spiradek: Zeitschrift für Werkstofftechnik 14 (1983) 417

/10/ Ph. Berge, J.R. Donate, D. Guttmann, P. Spiteri, L. Walibus: Memoires Scientifique Revue Metallurgie, November (1975) 837

/11/ H. Nahm, J. Moteff: Metallurgical Transactions 7A (1976) 1473

/12/ R.E. Villagrana, J.L. Kaae: Metallurgical Transactions 9A (1978) 527

/13/ A.A. Tavassoli, G. Colombe: Metallurgical Transactions 8A (1977) 1605

/14/ A.A. Tavassoli: Nuclear Engineering and Design 54 (1979) 279

/15/ K. La Malfa, S. Quaranta: in ref. 2, p. 71

/16/ A. Orlova, J. Cadek: Metal Science J. 15 (1981) 39

/17/ A. Plumtree, N.G. Persson: Metallurgical Transactions 7A (1976) 1743

/18/ N.G. Persson, L. Egnell: 2nd Meeting of Working Group of Alloy 800, Brussels, September (1976), paper 31

/19/ R.H. Cook: J. Nuclear Materials 66 (1977) 257

/20/ H. Fabritius, W. Wessling: Zeitschrift für Metalltechnik 11 (1980) 172

/21/ A. Czyrska-Filemonowicz, P.J. Ennis: Nuclear Technology 66 (1984) 149

/22/ W.B. Jones, R.M. Allen: Metallurgical Transactions 13 A (1982) 637

/23/ H. Aigner, M.P. Degischer, E. Hertner: Nuclear Technology 66 (1984) 54

/24/ M Vittori: Material Science J. 15 (1981) 3461

/25/ J.O. Nilsson: ibid 18 (1984) 351

/26/ V. Guttmann, R. Bürgel: ibid 17 (1983) 549

/27/ K. Schneider, W. Hartnagel, P. Schepp, B. Ilschner: Nuclear Technology 66 (1984) 289

/28/ K. Spiradek, H.P. Degischer, H. Lahodny: Proceedings of the Specialists' Meeting IAEA "High Temperature Metallic Materials For Gas-Cooled Reactors", Kraków, Poland 20-23 June 1988, ed. IAEA Vienna (1989) 54

/29/ R.v.d. Gracht, P.J. Ennis, A. Czyrska-Filemonowicz, W.J. Quadakkers, H. Schuster, H. Nickel: KFA Report, Jül-2211, KFA Jülich, Juni 1988

/30/ H.J. Grabke, A. Schnaas: in ref. 2, p. 195

/31/ A. Schnaas, H.J. Grabke: Werkstoffe und Korrosion 29 (9178) 635

/32/ P.J. Ennis, D.F. Lupton: in Proceedings of Petten Int. Conference on "Behaviour of High Temperature Alloys in Aggresive Environments", Petten, the Netherlands, 15-18 October 1979; eds. I. Kirman et al, The Metal Society of London (1980) 974

/33/ P.J. Ennis, D.F. Lupton, H. Nickel, H. Schuster: KFA Report, Jül-1786, KFA Jülich, May 1982

/34/ P.J. Ennis, K. Mohr, H. Schuster: Nuclear Technology 66 (9184) 363

/35/ M.E. Abd El-Azim, P.J. Ennis, H. Schuster, F.H. Hammad, H. Nickel: KFA Report, Jül-2344, KFA Jülich, January 1990

/36/ V. Guttmann, M. Schütze: in Proceedings of Int. Conference on "High Temperature Alloys for Gas Turbines and Other Aplications", Liège Belgium, 6-9 Oct. 1986; eds. W. Betz et al., D. Reidel Publishing Company, Dordrecht (1986) 293

/37/ H.M. Yun, P.J. Ennis, H. Nickel, H. Schuster:
J. Nuclear Materials 125 (1984) 258

/38/ J. Hemptenmacher, G. Sauthoff, H.J. Grabke:
Werkstoffe und Korrosion 35 (1984) 247

/39/ H.J. Grabke: in Proceedings First Polish-German Seminar on "Properties of High Temperature Alloys", Kraków Poland, 3-6 July 1985, Sc. Bulletins of Academy of Mining and Metallurgy, Chemistry No.5 (1987) 9

/40/ H. Schuster, M.H. Yun, P.J. Ennis, H. Nickel: ibid p. 35

/41/ V. Guttmann, K.E. Beck, R. Bürgel: Mat.-wiss. und Werkstofftechnik 19 (1988) 104

/42/ K. Spiradek: Korrelation zwischen Mikrostruktur und Kriechverformung des Legierungstyps X10 NiCrAlTi 32 20H (Alloy 800H), Dissertation, Montanuniversität, Leoben, Austria 1987

/43/ J. Beach, D.H. Warrington: J. Iron and Steel Institute 204 (1966) 460

/44/ W. Dudzinski, J.P. Mornirolli, M. Gantois: J. Materials Science 15 (1980) 1387

/45/ J.P. Mornirolli, M. Gantois: J. Applied Crystallography 16 (1983) 1

/46/ E. Bauer-Grosse, J.P. Mornirolli, G. Le Caer: Acta Metallurgica 29 (1981) 1983

/47/ A. Czyrska-Filemonowicz, K. Spiradek, S. Gorczyca: Proceedings of 8.Int. Metallographie-Tagung, 10.-13. Oktober 1990, Leoben, Austria, Praktische Metallographie 22 (1991) 217

/48/ W. J. Quadakkers, H. Schuster: Werkstoffe und Korrosion, 36, 1985, 141-150

/49/ W. J. Quadakkers, ibid, 36, 1985, 335-347

/50/ R. Schulten, K. Bongartz, W. J. Quadakkers, H. Schuster, H. Nickel: Report of the KFA Jülich Jül-2319, Nov 1989.

Table I: Details of the Test Materials

Alloy producer	Vereinigte Deutsche Metallwerke
Designation	Nicrofer 3220H
Heat number	74602
Form and heat treatment	22 mm diam forged bar, solution treatment at 1150 °C
Chemical Analysis (wt%)	
Carbon	0.064 (0,075*)
Manganese	0.85
Silicon	0.32
Chromium	20.55
Nickel	31.00
Sulphur	0.003
Phosphorus	0.015
Titanium	0.35
Aluminium	0.25
Nitrogen	0.015*
Iron	Balance

Table II: Specimens selected for SEM

	Specimen Number	Heat treatment	Impact test temperature, °C
A2-1	AHZ 141	ST+850 °C/500h/air (in argon)	RT
A2-2	AHZ 147	-"-	400
A2-3	AHZ 144	-"-	600
A2-4	AHZ 150	-"-	800
B2-1	AHZ 39	St+850°C/500h/air in argon-10% CH_4	RT
B2-2	AHZ 45	-"-	400
B2-3	AHZ 42	-"-	600
B2-4	AHZ 48	-"-	800
C-4	AHZ 82	ST+ carburized at 850°C/500h+ +heated at 900°C/ 500h	800

* determined at KFA - all other values from the manufacture's certification

Table III: Specimen selected for TEM		
	Specimen Number	Heat treatment*
0	AHZ 3	ST
A1	AHZ 117	ST + A(100h)
A2	AHZ 141	ST + A(500h)
B1	AHZ 15	ST + C(100h)
B2	AHZ 37	ST + C(500h)
C	AHZ 73	ST + C(500h) + heating at 900°C/500h

* ST: solution treatment at 1150°C for 0,5h followed by water quenching

A: ageing at 850°C for 100 or 500h, followed by air cooling

C: carburization at 850°C for 100 or 500h in argon - 10% vol% CH_4

Table IV: Results of impact tests and bulk carbon analysis

Specimen No.	Condition	Test temp. °C	Measured Impact energy J			Average Impact energy J	Bulk carbon content (w%)			
1 - 3	solution treated	25	230+	227+	231	229	0.067	0.068		
7 - 9		400	196+	(170+)	199+	198				
4 - 6		600	(164+)	195+	194+	194	0.066	0.066		
10 - 12		800	202+	216	212+	210				
115 - 117	St + 100 h/850 °C	25	139	148	150	146	0.066		0.068	
121 - 123	in argon	400	193	181	190	188				
118 - 120		600	164	154	160	159	0.066		0.066	
124 - 126		800	185	184	17	182				
127 - 129	St + 250 h/850 °C	25	156	154	155	155	0.065		0.067	
133 - 135	in argon	400	(218)	180	184	182				
130 - 132		600	179	173	(147)	176	0.066		0.066	
136 - 138		800	187+	191	184	187				
139 - 141	St + 500 h/850 °C	25	154	150	143	149			0.066	0.066
145 - 147	in argon	400	203	198	196	199				
142 - 144		600	169	167	162	166			0.066	0.066

Table IV: Results of impact tests and bulk carbon analysis **(continued)**

Specimen No.	Condition	Test temp. °C	Measured Impact energy J			Average Impact energy J	Bulk carbon content (w%) Specimen No.	
148 - 150		800	189	199+	199+	196		
13 - 15*	St + 100 h/850 °C	25	147	173	161	160	0.09	0.09
19 - 21	in argon	400	190	196	186	191	0.12	0.11
16 - 18		600	160	163	151	158	0.11	0.11
22 - 24		800	167	156	162	162	0.10	0.10
25 - 27	St + 250 h/850 °C	25	103	104	107	105	0.30	0.29
31 - 33	in argon-10 % CH_4	400	124	119	121	121	0.24	0.24
28 - 30		600	106	108	101	105	0.34	0.34
34 - 36		800	110	116	115	114	0.32	0.33
37* - 39	St + 100 h/850 °C	25	59	60	59	59	0.63	0.64
43 - 45	in argon-10 % CH_4	400	67	66	63	65	0.24	0.24
40 - 42		600	64	60	59	60	0.55	0.59
46 - 48		800	(70)	58	61	60	0.55	0.54
49 - 51	St + 100 h/850 °C	25	134	122	130	129	0.10	0.10
55 - 57	in argon-10 % CH_4	400	171	183	171	175	0.08	0.08
52 - 54	+ 500 h/900 °C in	600	136	150	131	139	0.12	0.10
58 - 60	argon	800	160	164	164	163	0.09	0.09

Table IV: Results of impact tests and bulk carbon analysis **(continued)**

Specimen No.	Condition	Test temp. °C	Measured Impact energy J			Average Impact energy J	Bulk carbon content (w%) Specimen No.	
61 - 63	St + 250 h/850 °C	25	62	60	80	67	0.38	0.38
67 - 69	In argon-10 % CH_4	400	94	74	82	83	0.23	0.23
64 - 66	+ 500 h/900 °C	600	78	90	77	82	0.29	0.30
70 - 72	In argon	800	94	81	85	87		
73*- 75	St + 500 h/850 °C	25	43	43	41	42	0.62	0.64
79 - 81	In argon-10 % CH_4	400	52	50	52	51	0.62	0.62
76 - 78	+ 500 h/900 °C	800	45	51	47	48	0.59	0.63
82 - 84	In argon	800	47	48	46	47	0.54	0.55

Footnotes : + specimen not completely fractured

( ) values not considered in calculating average impact energy

* specimen selected for TEM investigations

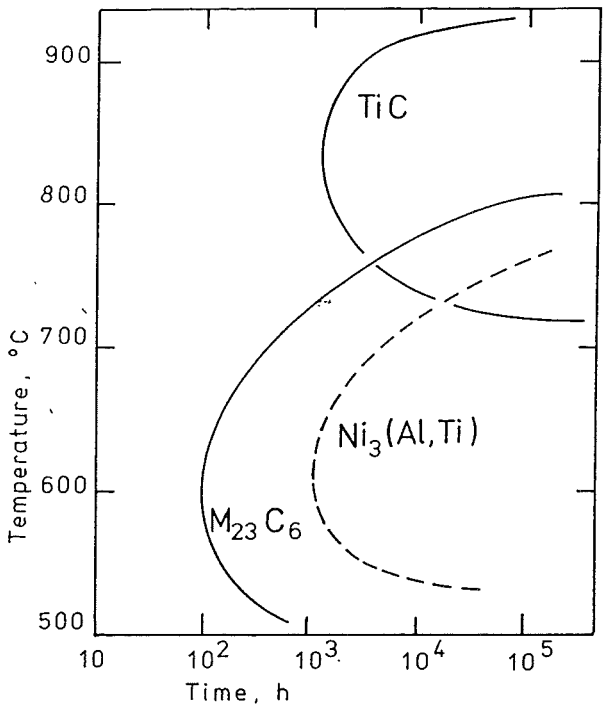

Fig. 1: Time-temperature-precipitation diagram for Alloy 800; Orr /5/.

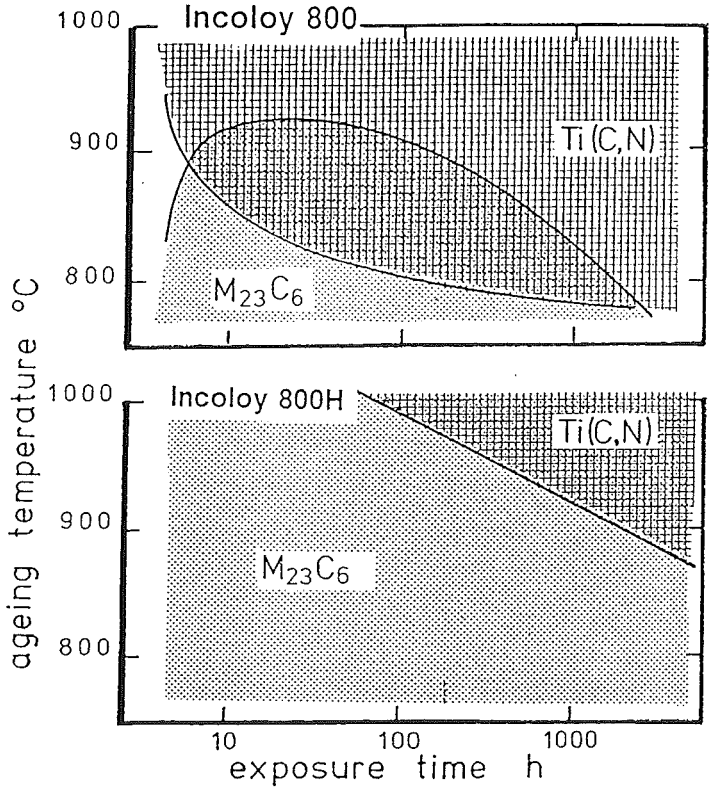

Fig. 2: Schematic diagram of precipitation behaviour of Alloy 800 (C = 0.033 %; Ti = 0.32 %) and Alloy 800H (C = 0.078 %; Ti = 0.3 %) at high temperatures; Degischer and Aigner /6/.

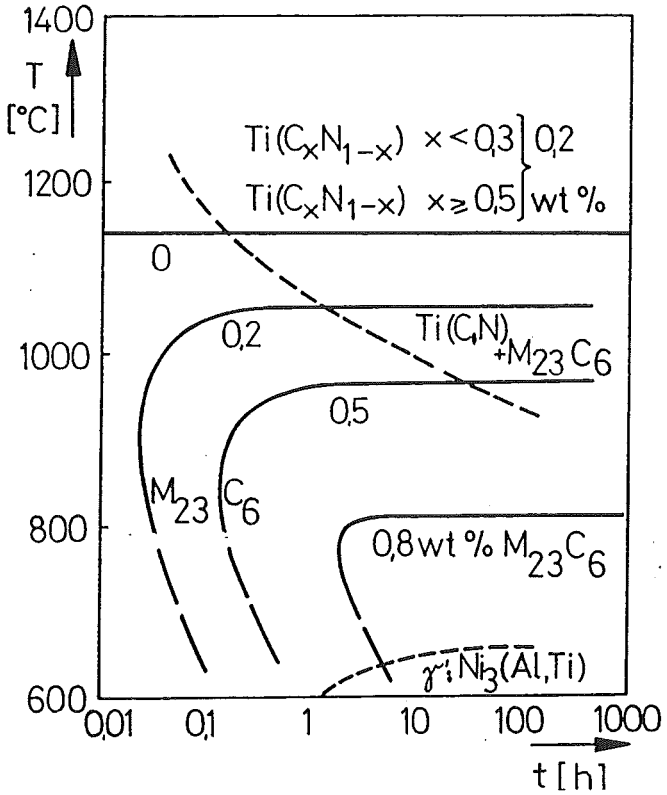

Fig. 3: Time-temperature-precipitation diagram for Alloy 800H (C = 0,078 %; Ti = 0,3 %) aged at high temperatures; Degischer et al /7/.

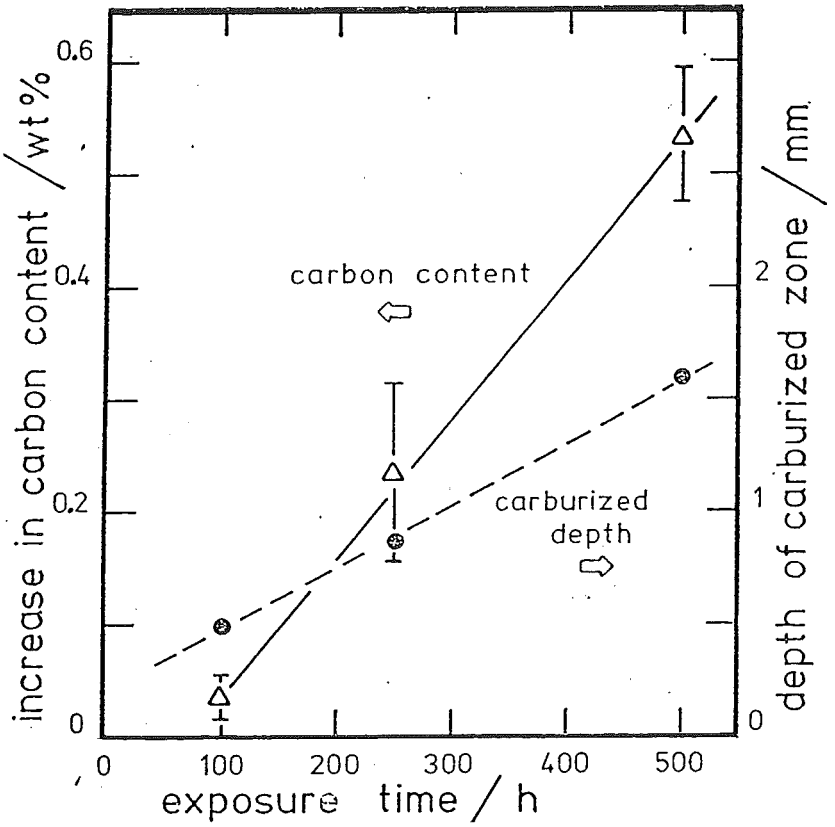

Fig. 4: Carbon uptake rate and depth of carburized zone (continuous grain boundary carbides) for Alloy 800H carburized in Ar-10 vol % CH_4 at 850 °C.

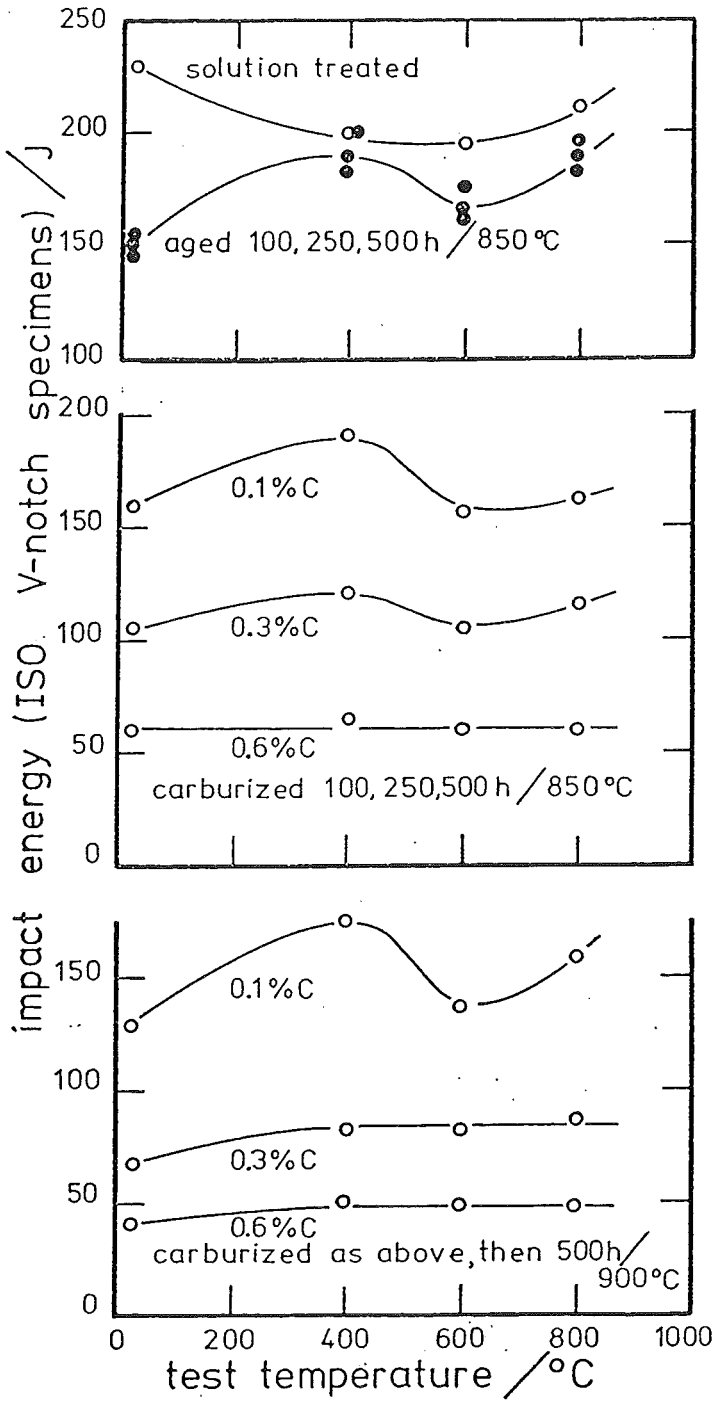

Fig. 5: Impact energy of Alloy 800H at test temperatures of 20 - 800 °C after various heat treatments. The bulk carbon contents (wt %) of the specimens are indicated.

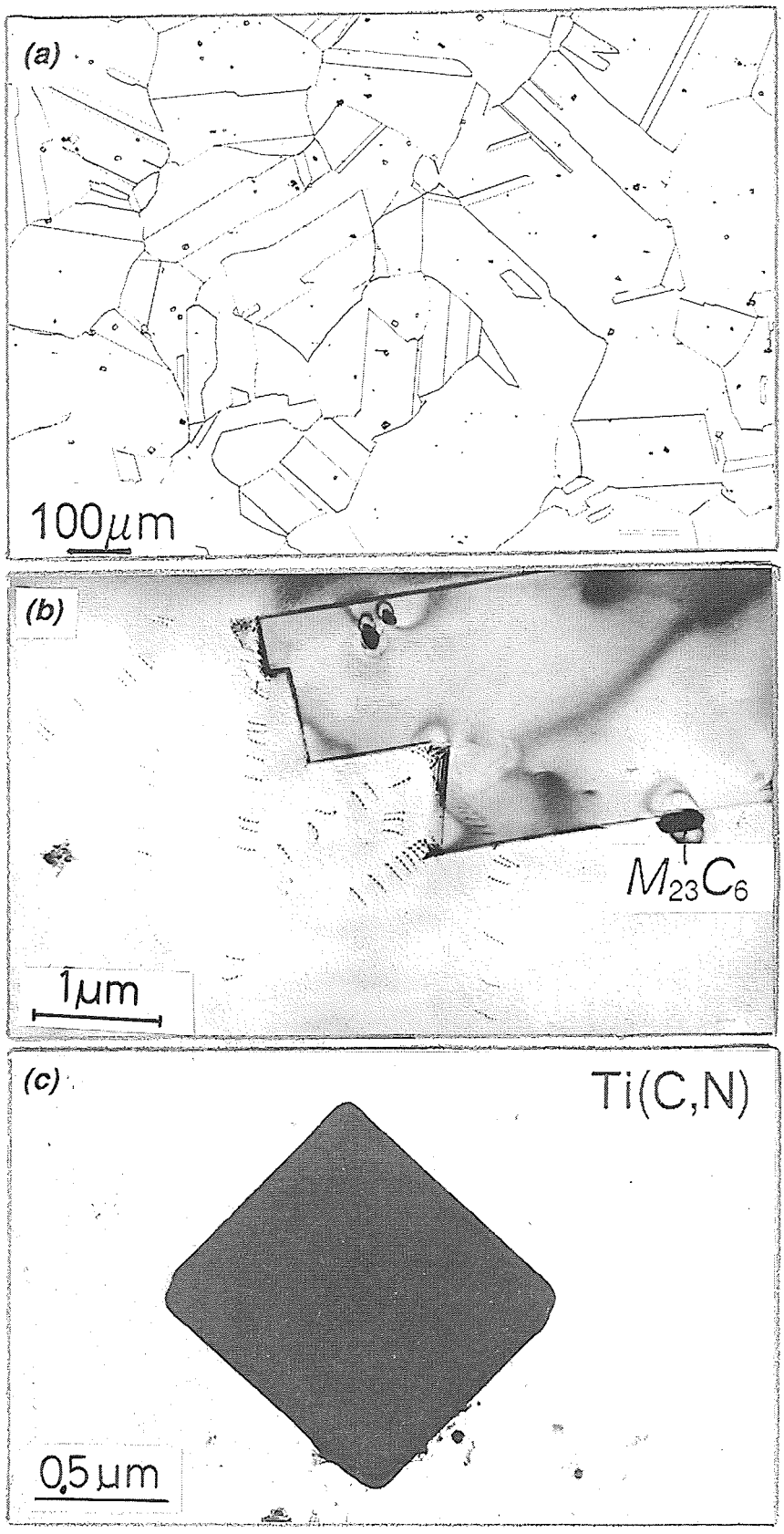

Fig. 6: As-received material
Microstructure of Alloy 800 H solution treated at 1150 °C (0,5h) w.q. examined by optical microscopy (Fig.a) and by TEM (Fig.b, c).

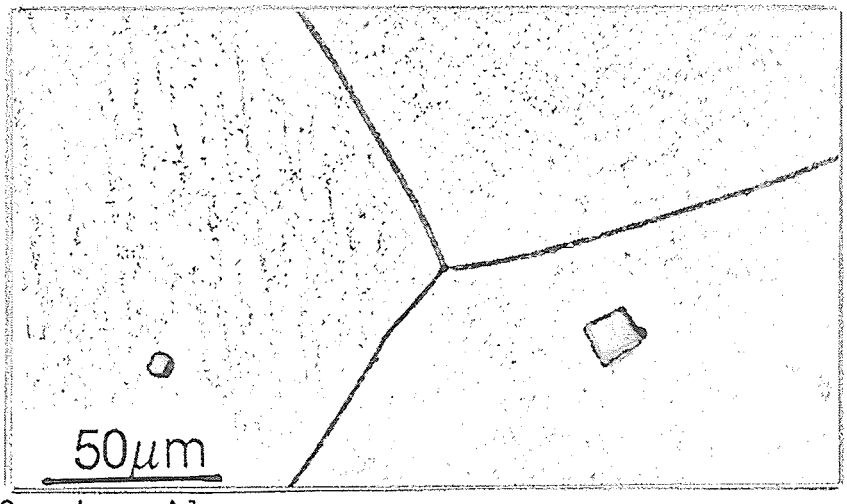

Fig. 7: Specimen A1
Microstructure of Alloy 800H aged at 850 °C for 100 h revealed by optical microscopy.

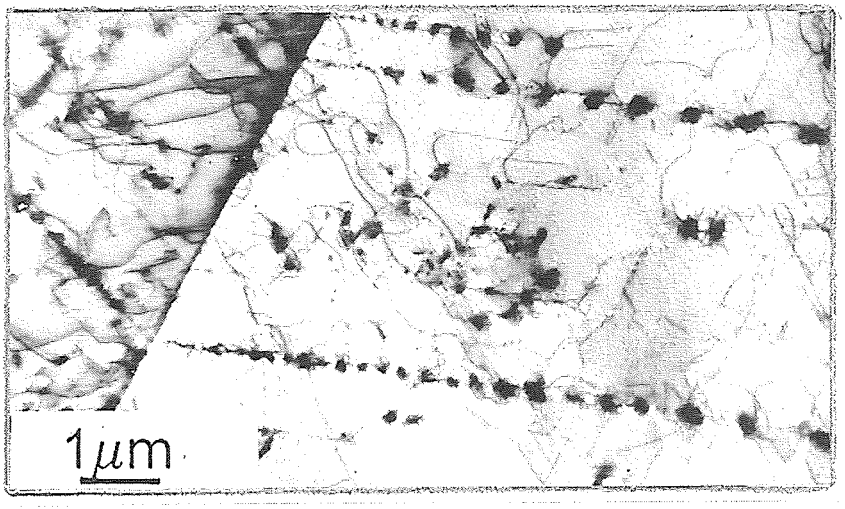

Fig. 8: Specimen A1
Intragranular precipitation of $M_{23}C_6$ carbides

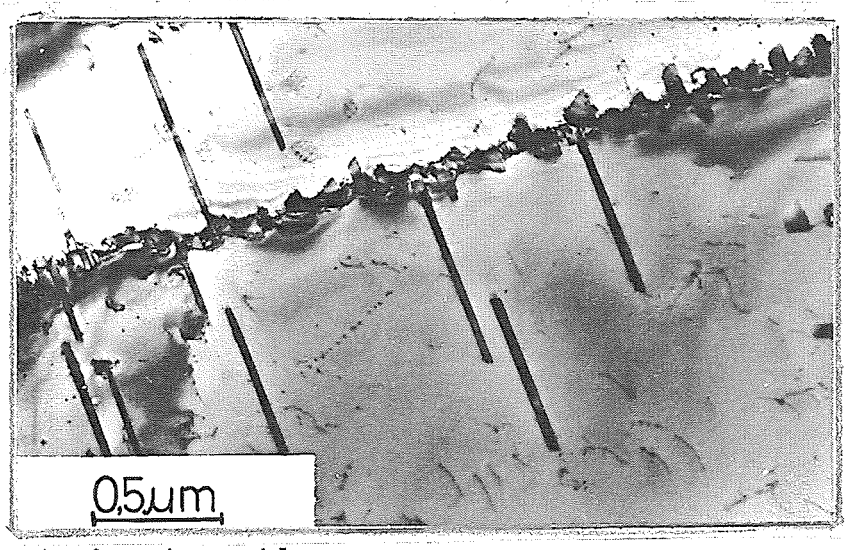

Fig. 9: Specimen A1
$M_{23}C_6$ carbides precipitated on non-coherent twin boundary

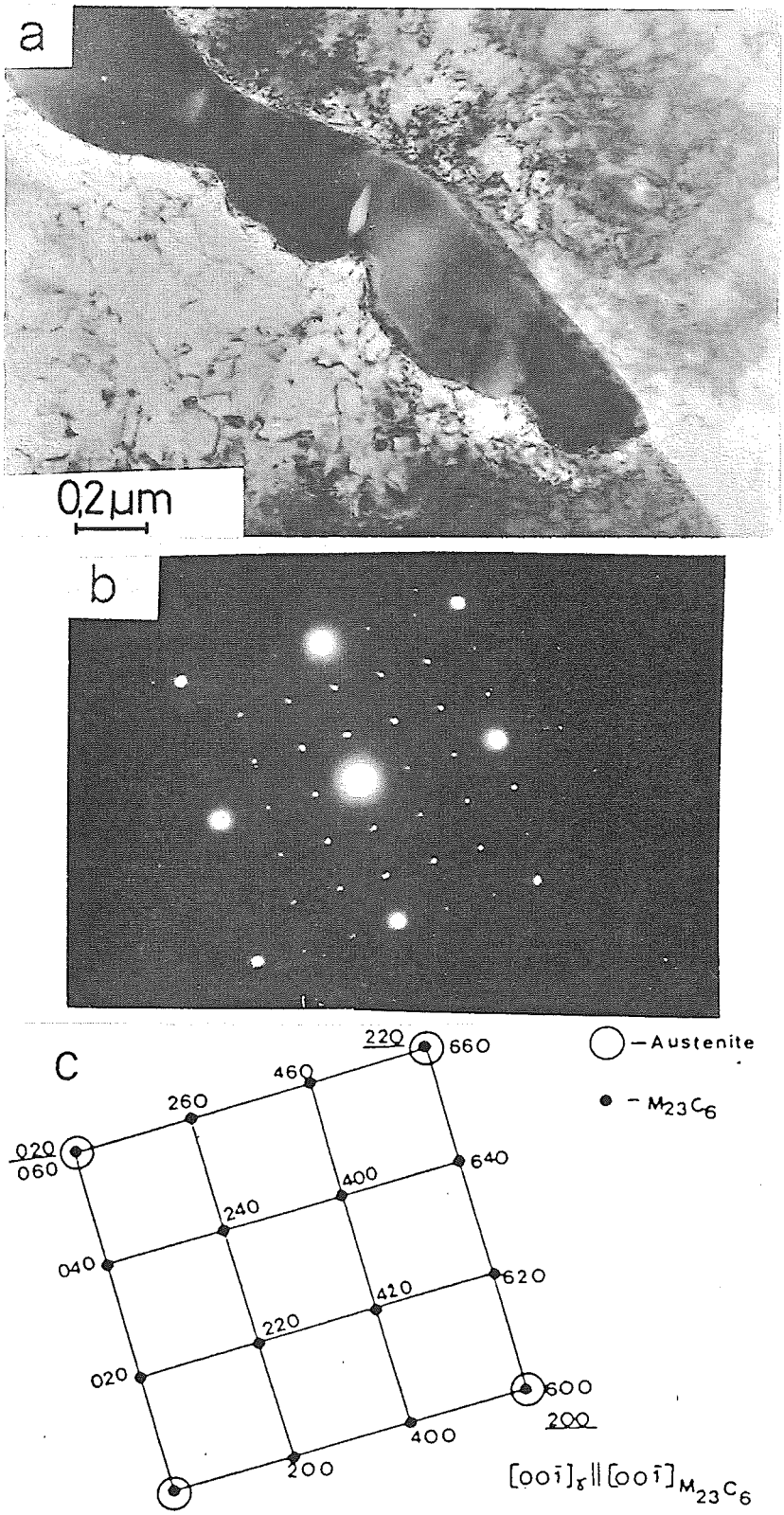

Fig. 10: Specimen A1

Grain boundary $M_{23}C_6$ carbides (Fig.a) grow with parallel orientation to the matrix (Fig.b, c).

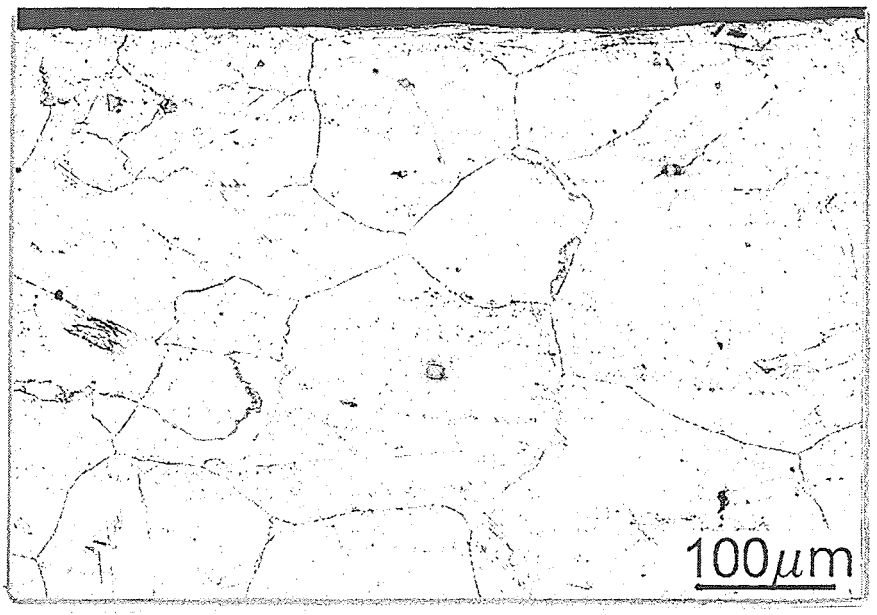

Fig. 11: Specimen A2
Microstructure of Alloy 800H aged at 850 °C for 500 h revealed by optical microscopy.

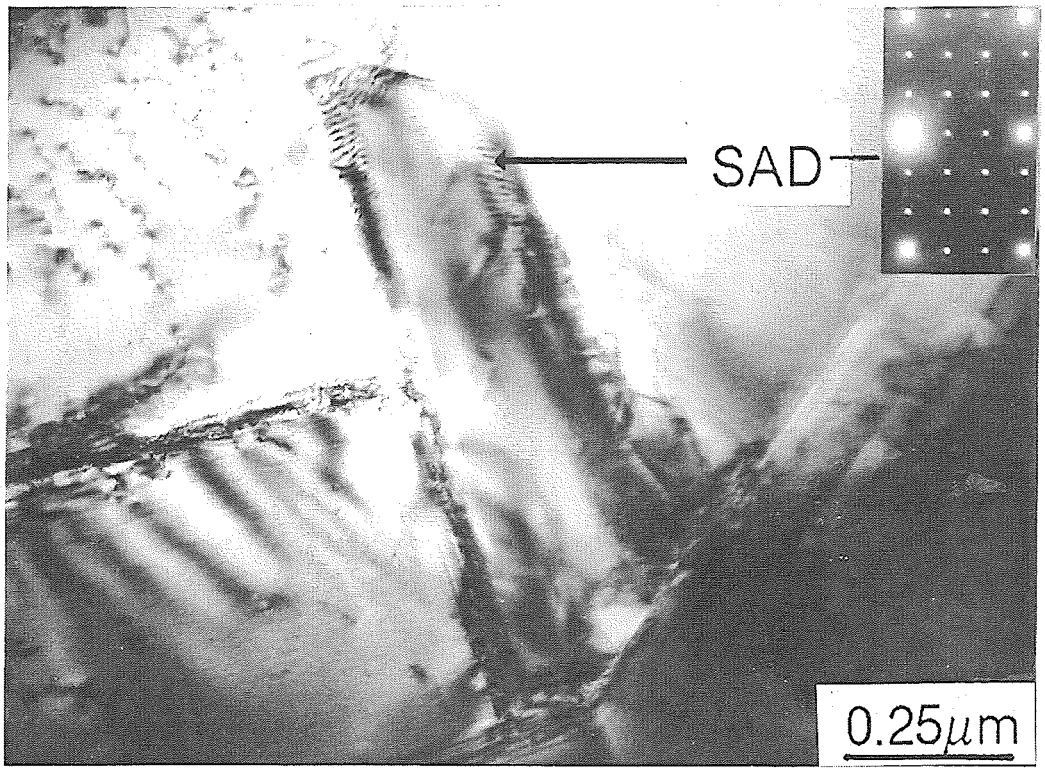

Fig. 12: Specimen A2
$M_{23}C_6$ grows at a triple grain boundary junction. Electron diffraction pattern (SAD) shows the parallel orientation of $M_{23}C_6$ and γ lattices.

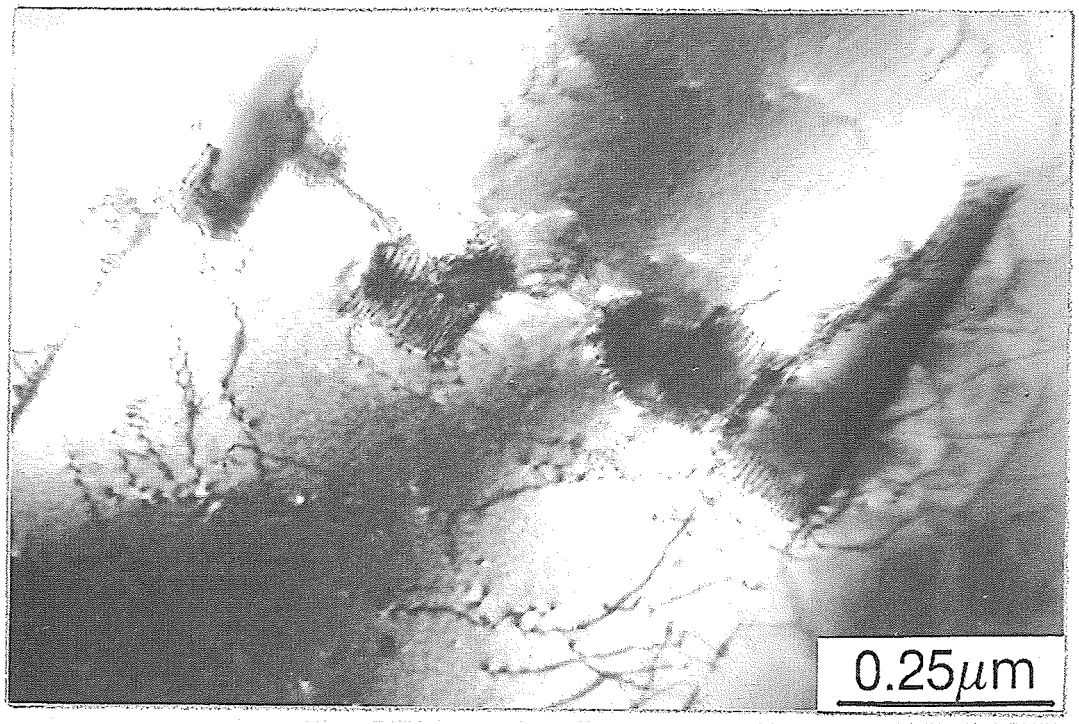

Fig. 13: Specimen A2
$M_{23}C_6$ carbides precipitated on non-coherent grain boundary parallel to the twinning plane.

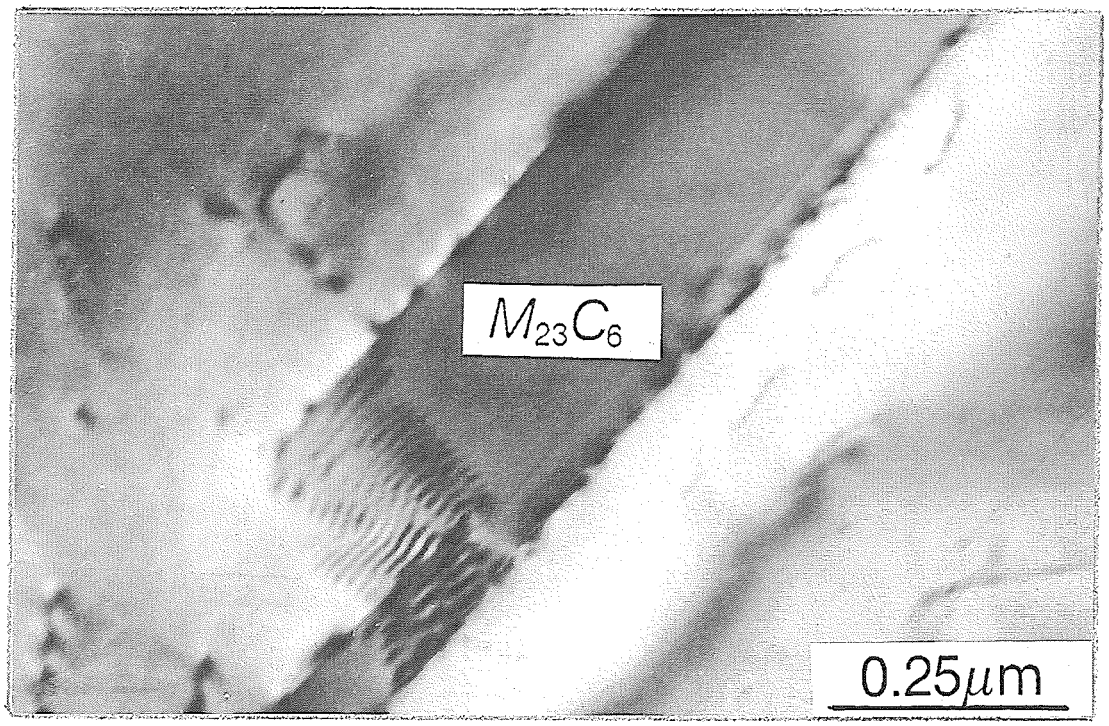

Fig. 14: Specimen A2
$M_{23}C_6$ carbides precipitated on coherent twin boundary growing along the twinning plane.

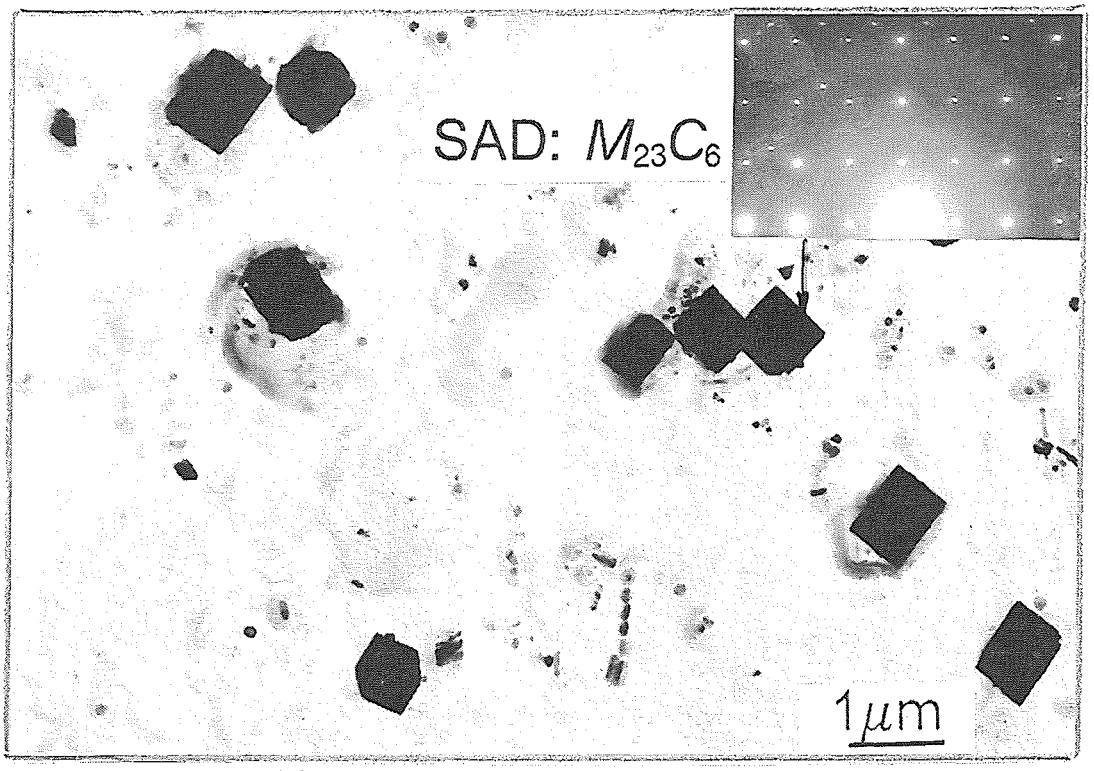

Fig. 15: Specimen A2
Intragranular precipitation of $M_{23}C_6$ carbides (extraction double-replica).

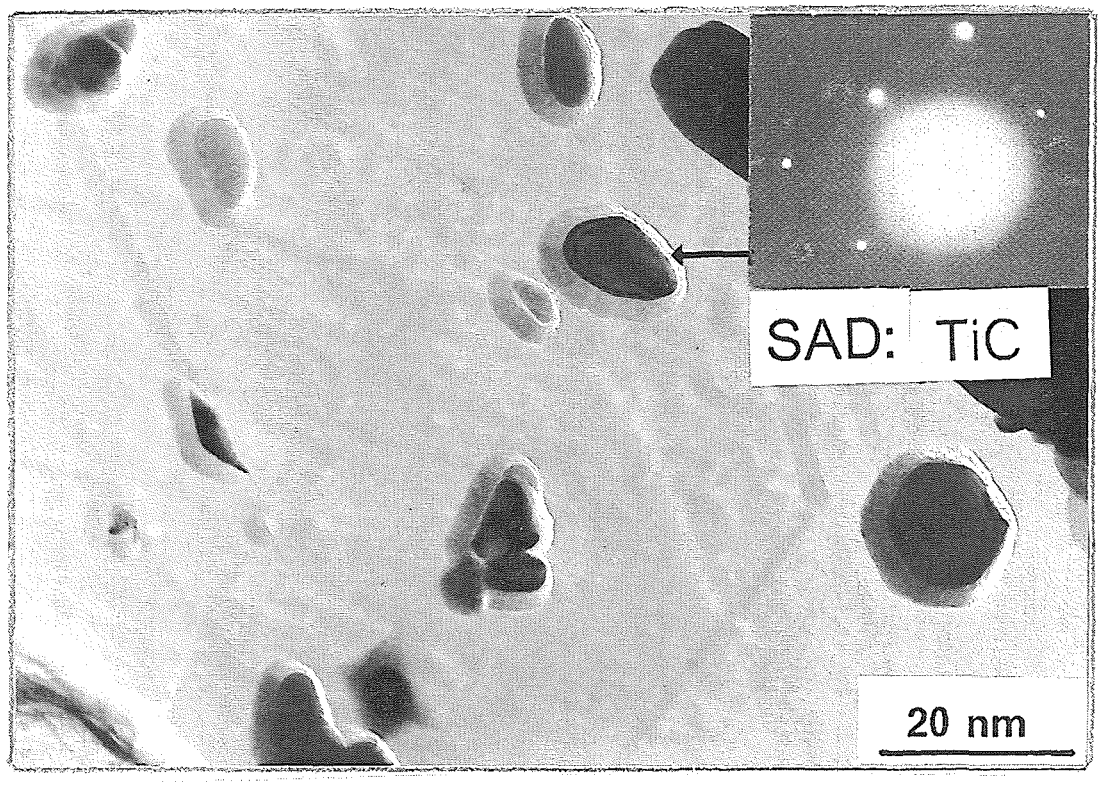

Fig. 16: Specimen A2
Fine secondary TiC extracted on the replica.

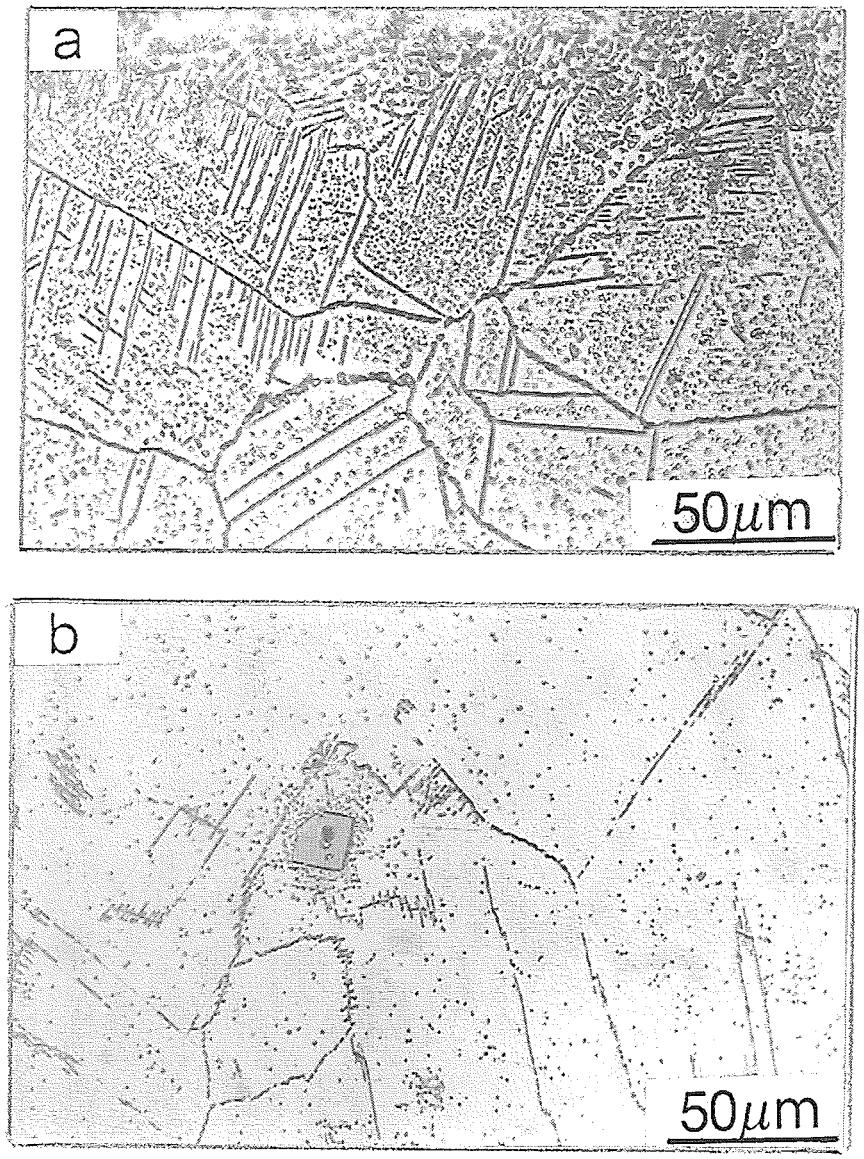

Fig. 17: Specimen B1
Microstructure of the alloy carburized at 850 °C for 100h in argon-10 % methane; carburized zone (Fig.a) and non-carburized core (Fig.b).

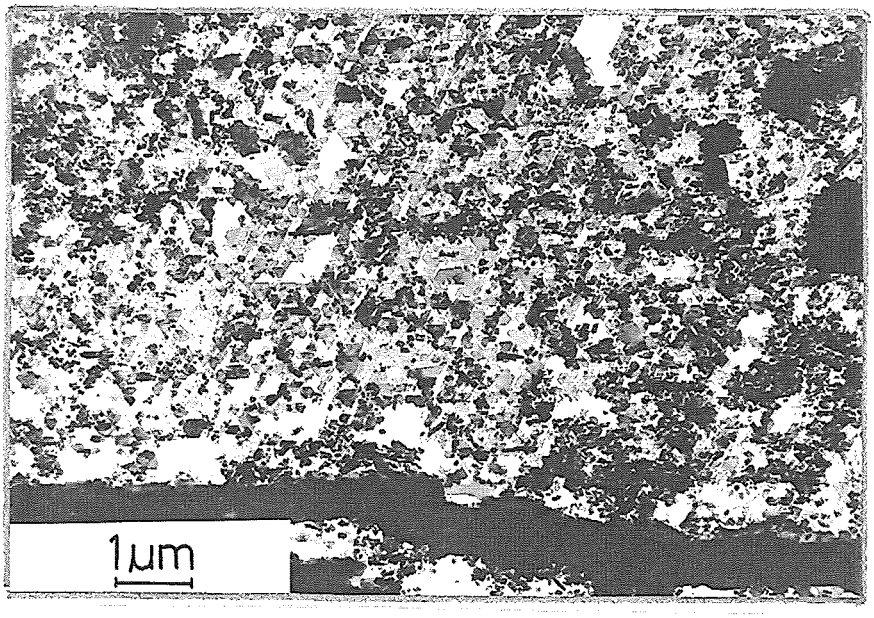

Fig. 18: Specimen B1 - carburized zone
Morphology of $M_{23}C_6$ carbides.

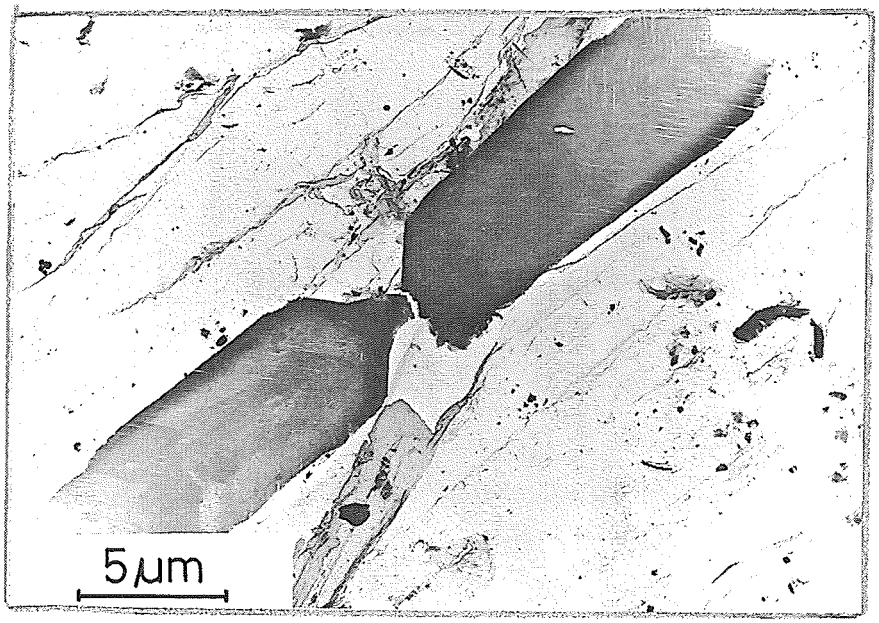

Fig. 19: Specimen B1 - carburized zone
Large M_7C_3 carbides extracted on the replica.

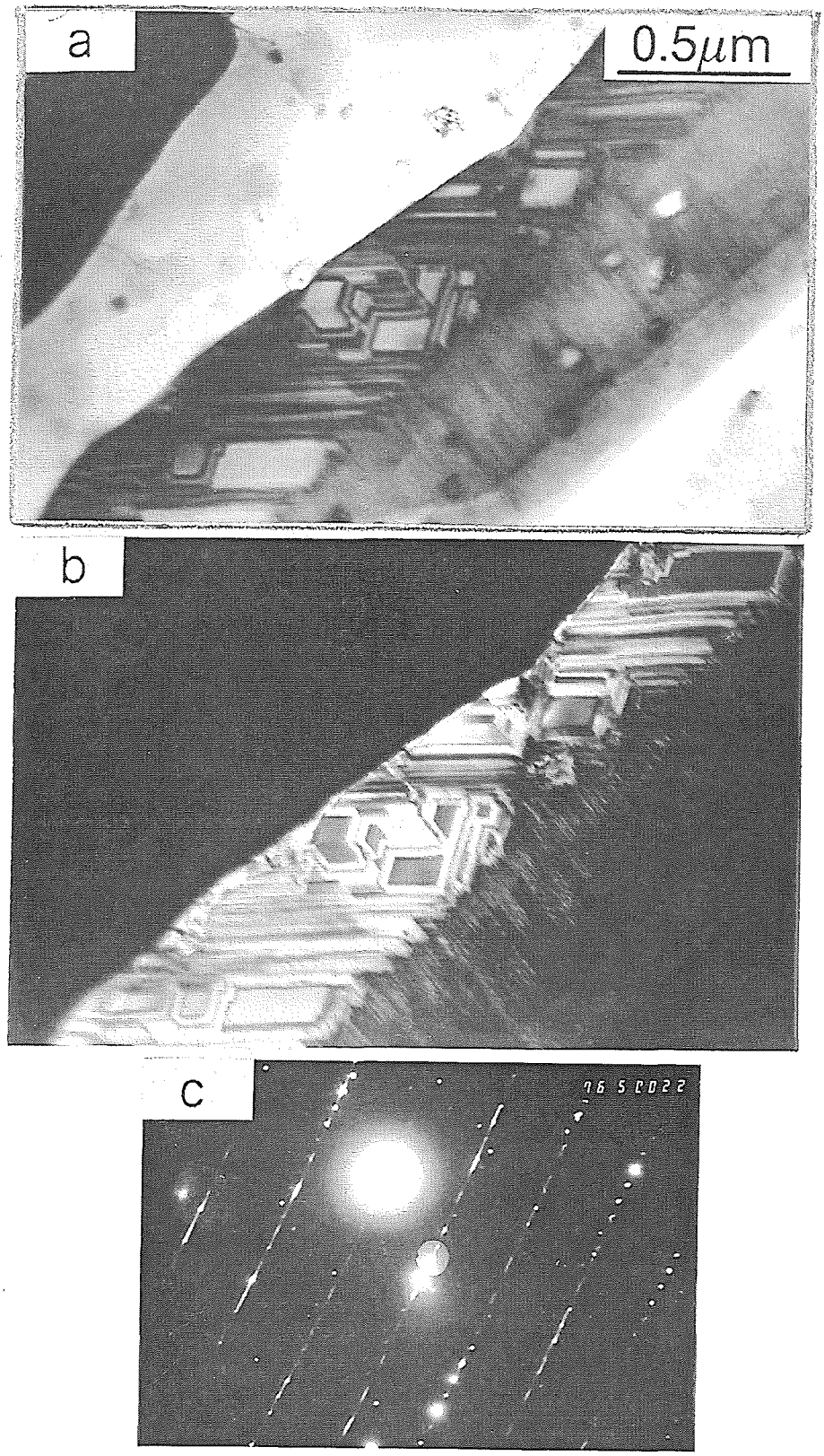

Fig. 20: Specimen B1 - carburized zone
M_7C_3 carbide with planar defects revealed by TEM in bright-field (a) and dark-field (b) images. Electron diffraction pattern shows characteristic streaks (c).

Fig. 21: Specimen B2
Microstructure of the alloy carburized at 850 °C for 500 h in argon-10 % methane revealed by optical microscoy.

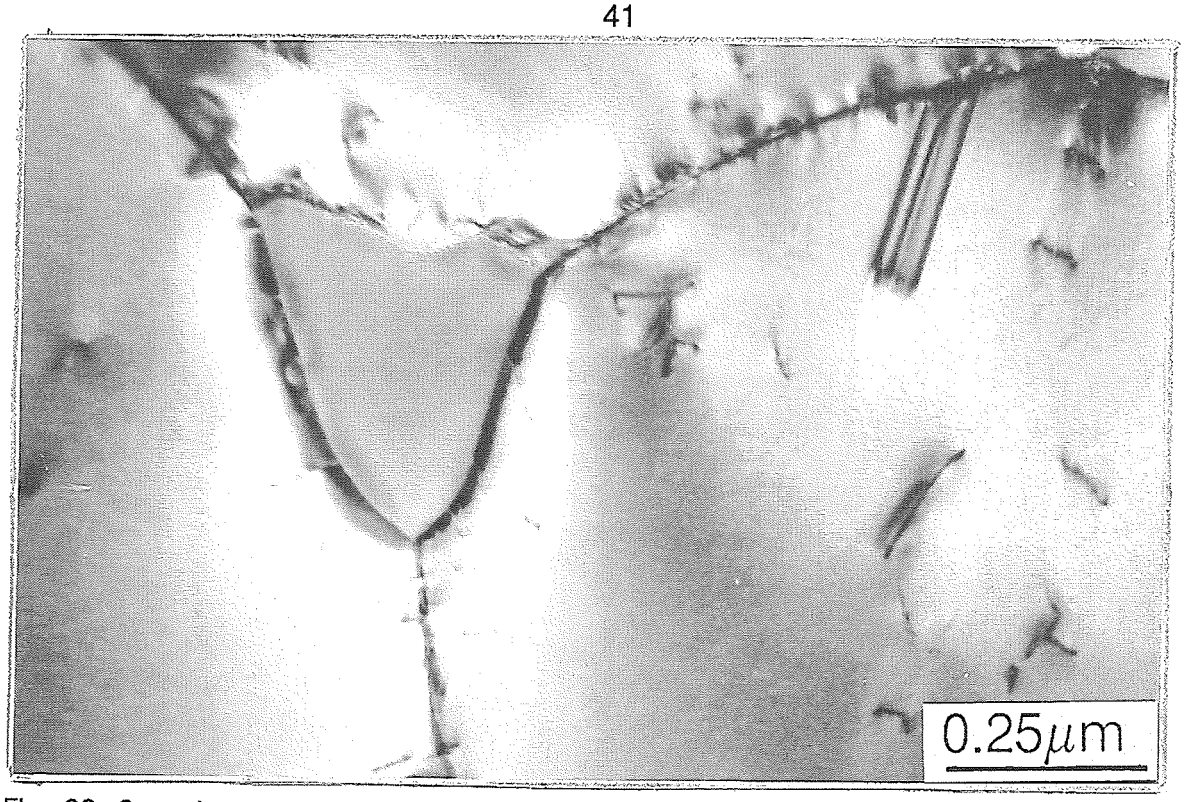

Fig. 22: Specimen B2
$M_{23}C_6$ carbide precipitated at the junction of three grains (thin foil).

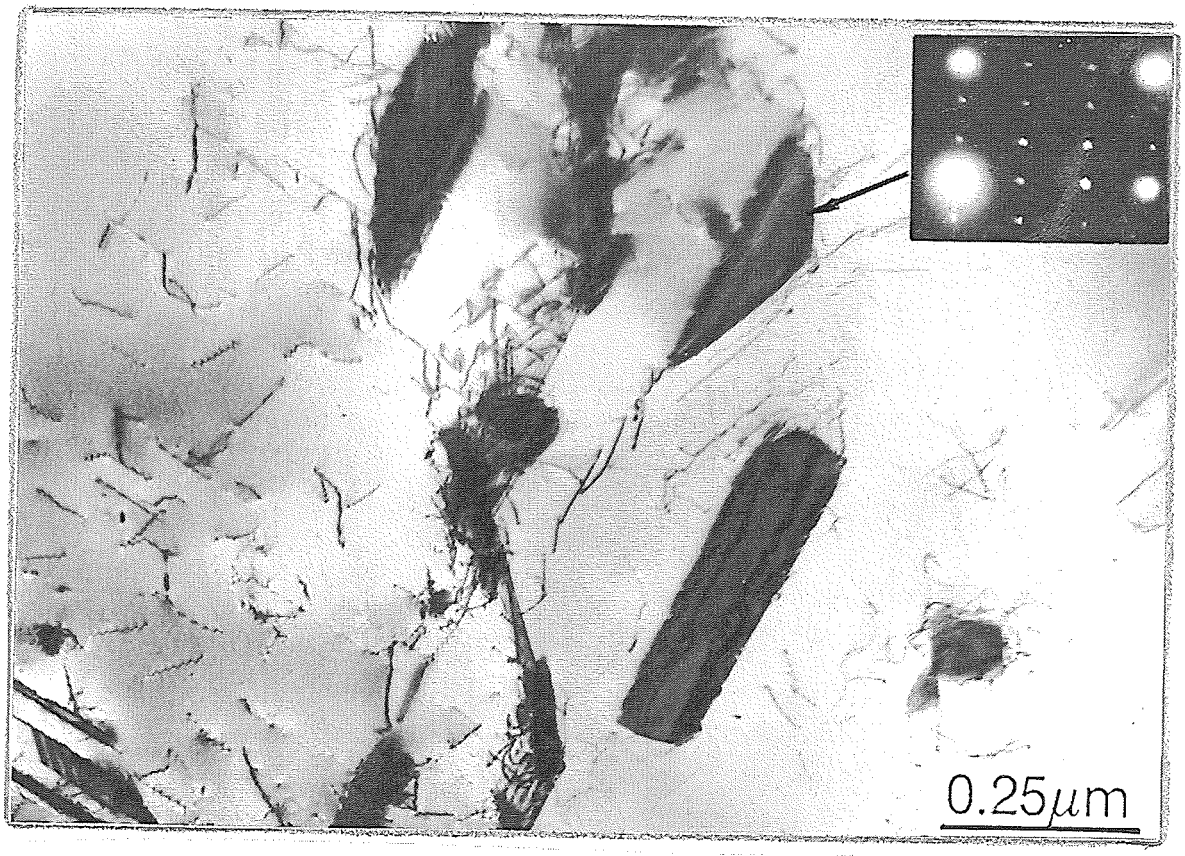

Fig. 23: Specimen B2
Precipitation on twin boundaries and the vicinity of twin boundary (thin foil).

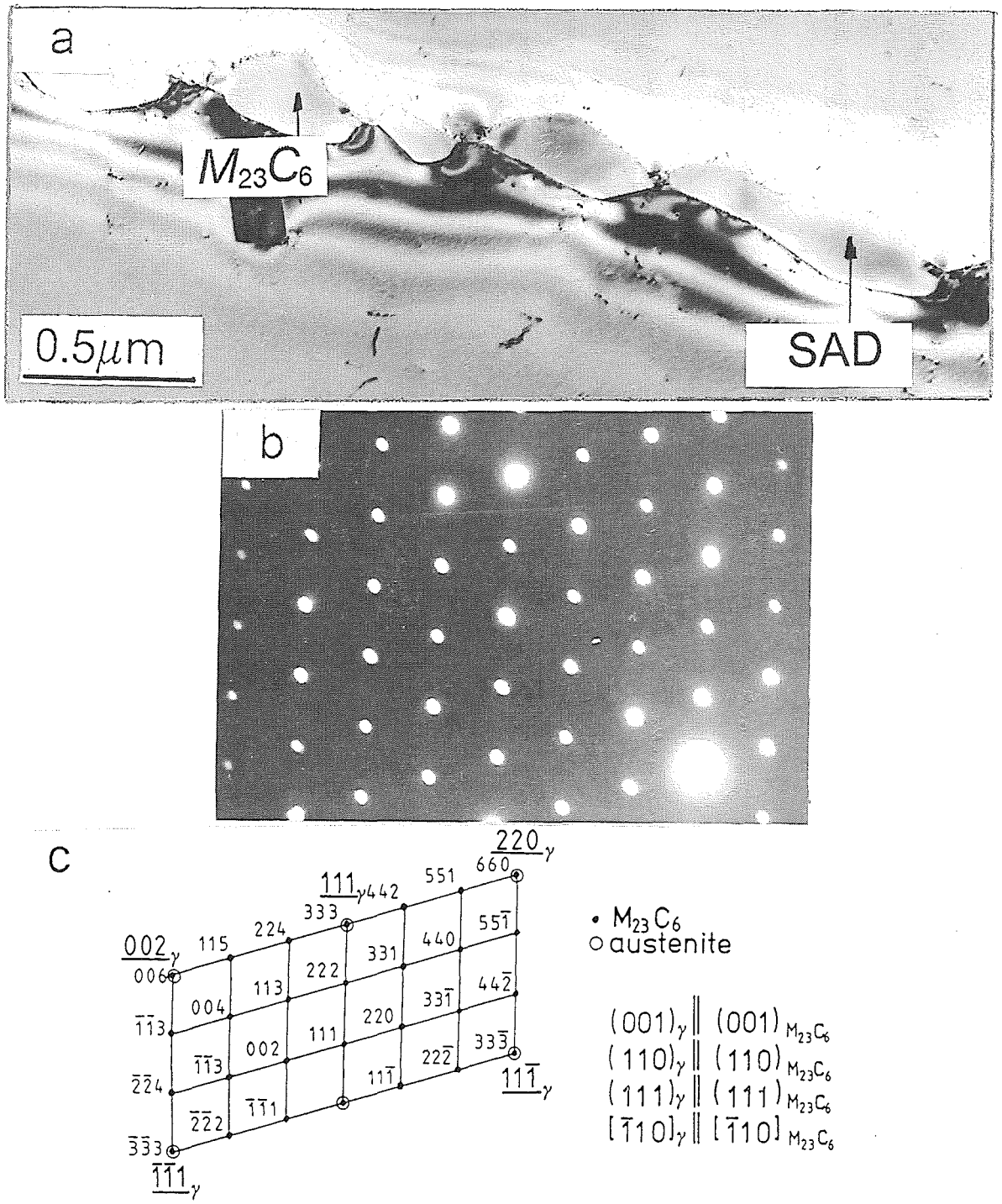

Fig. 24: Specimen B2

a) $M_{23}C_6$ carbides precipitated on the grain boundary (thin foil)
b) Electron diffraction pattern showing parallel orientation of matrix (intense spots) and $M_{23}C_6$ carbide (faint spots) presented on Fig. a.
c) Crystallographic relation between the two phases.

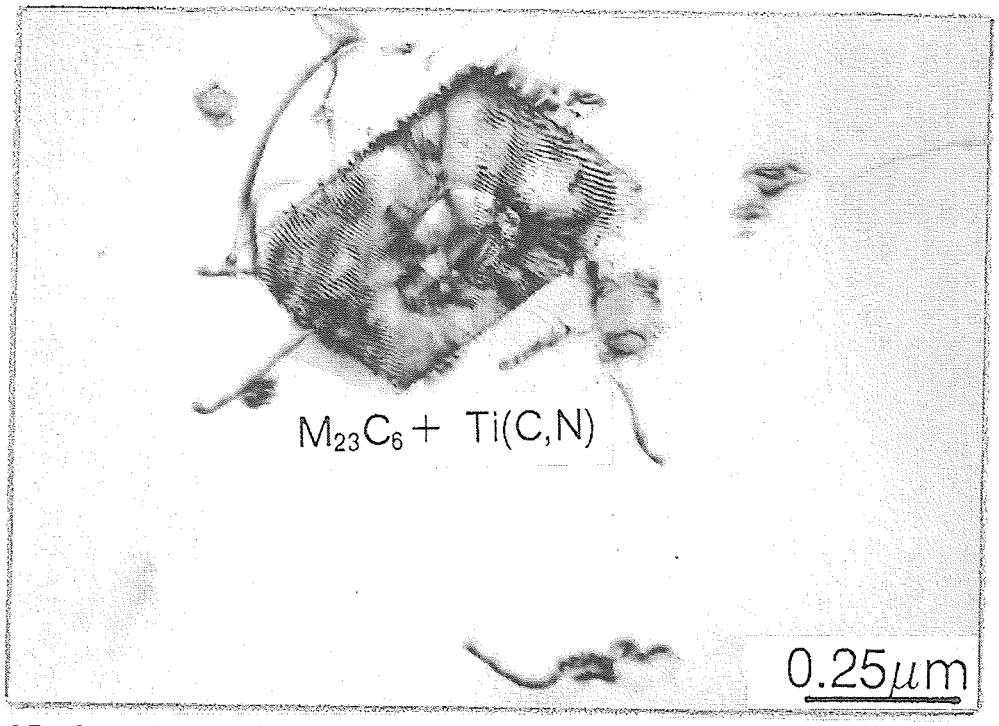

Fig.25: Specimen B2
Chromium-rich $M_{23}C_6$ carbide precipitated at primary titanium carbonitride.

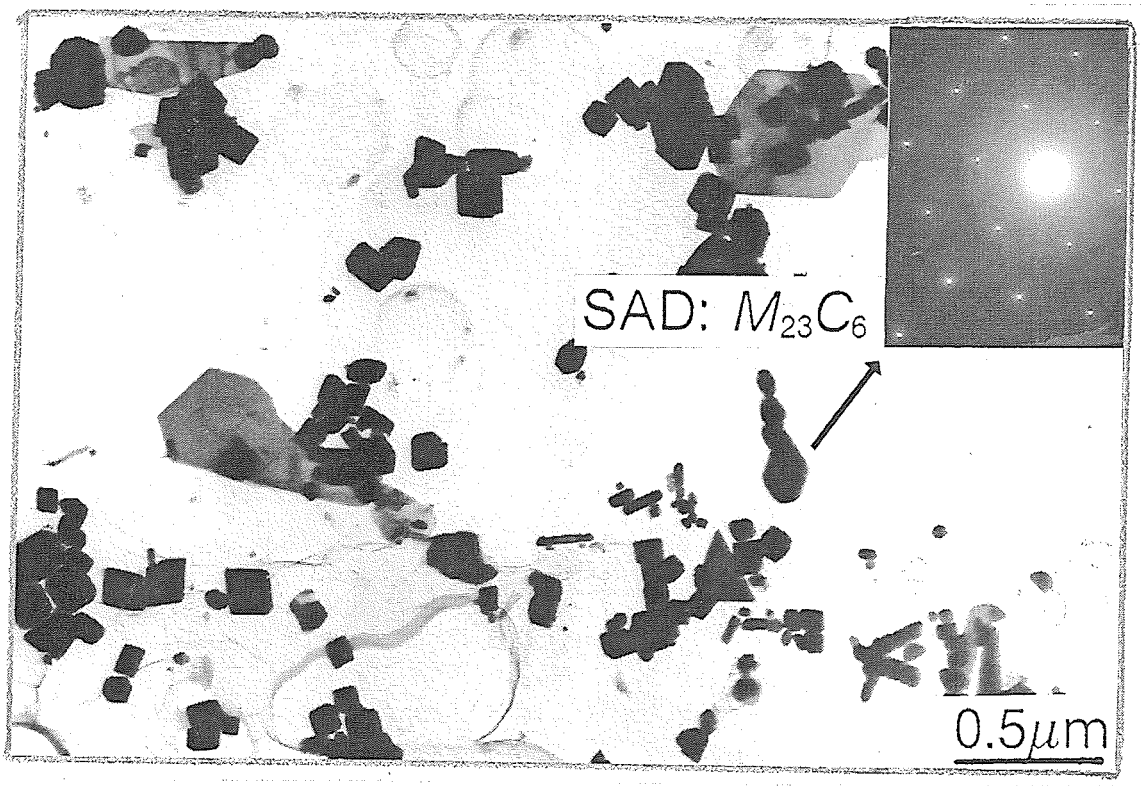

Fig.26: Specimen B2
The morphology of $M_{23}C_6$ carbides observed on the extraction replica.

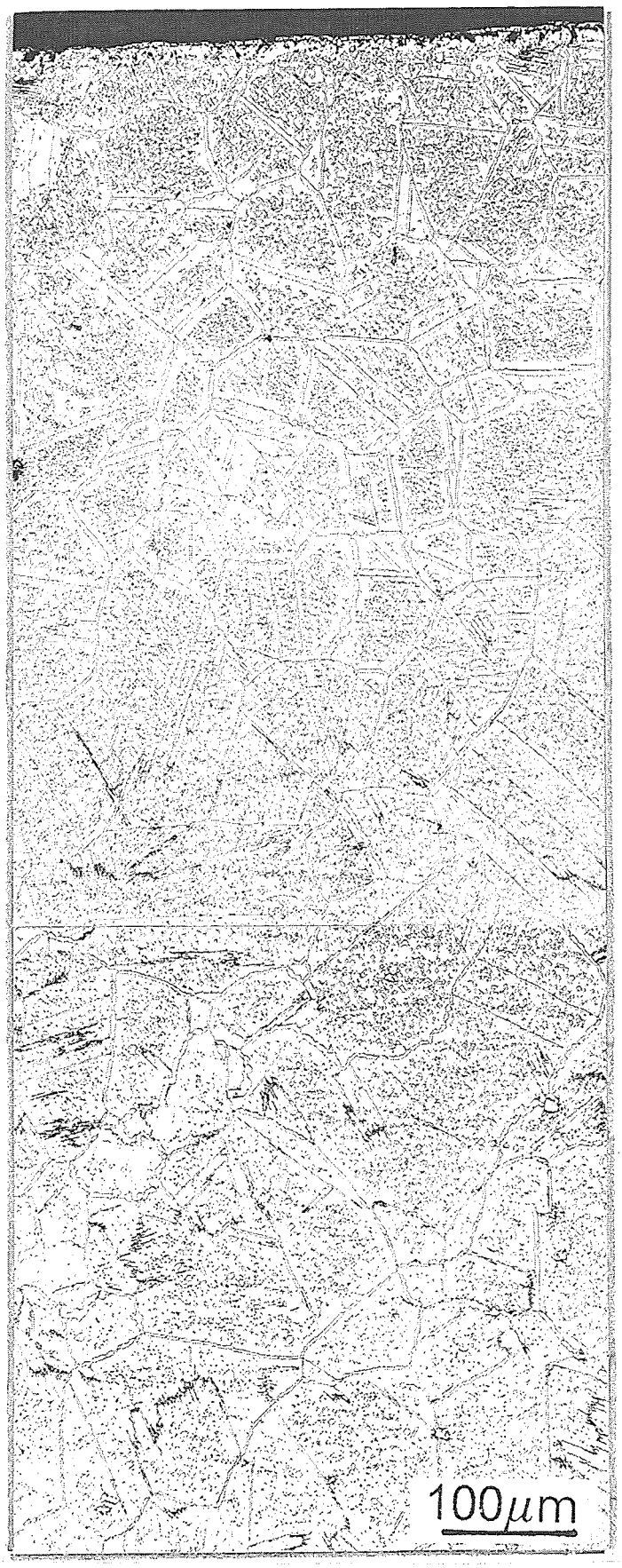

Fig.27: Specimen C
Microstructure of the alloy heated at 950 °C for 500 h after carburization treatment.

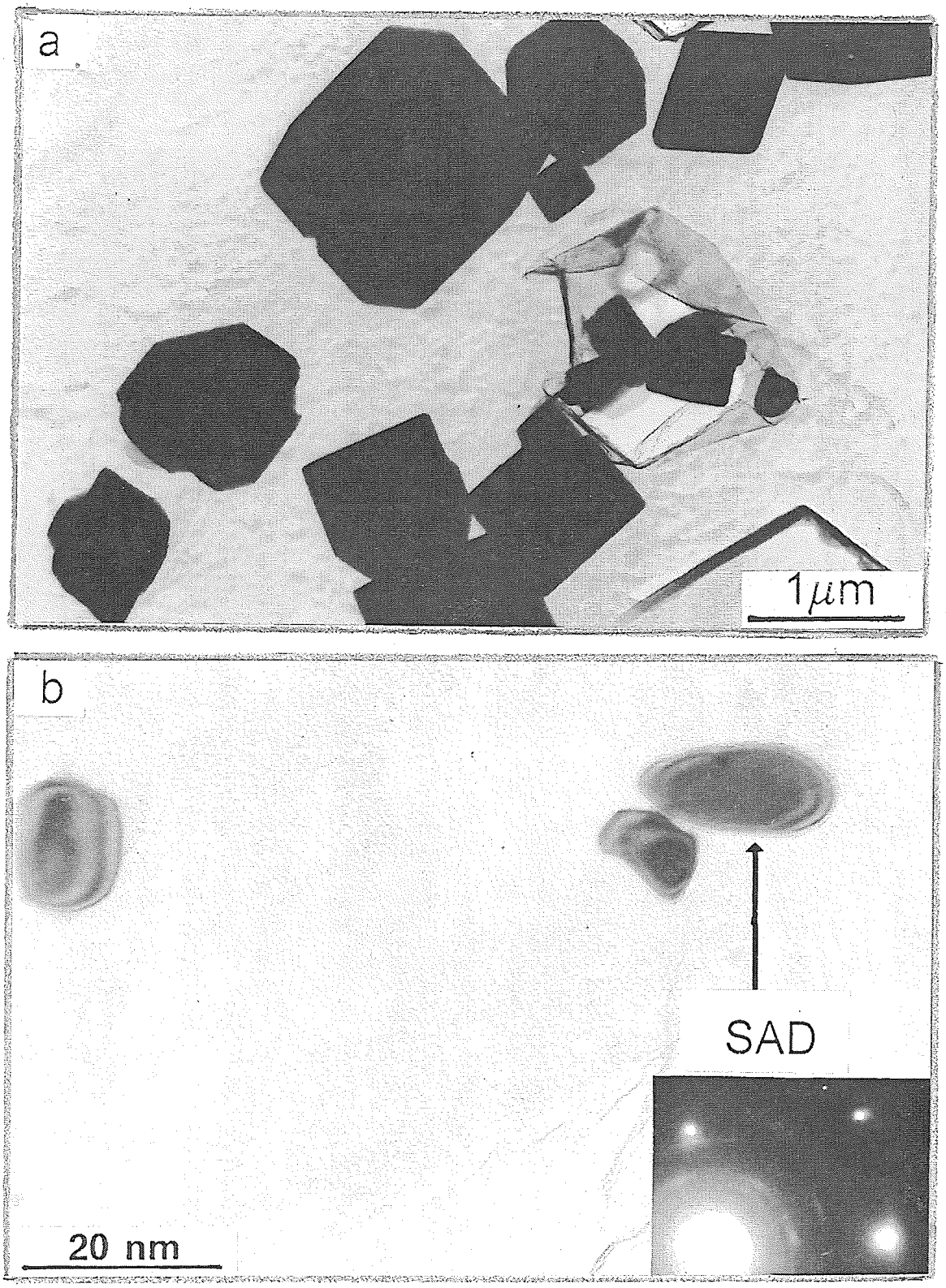

Fig.28: Specimen C
Morphology of intragranular $M_{23}C_6$ (Fig.a) and TiC (Fig.b) carbides.

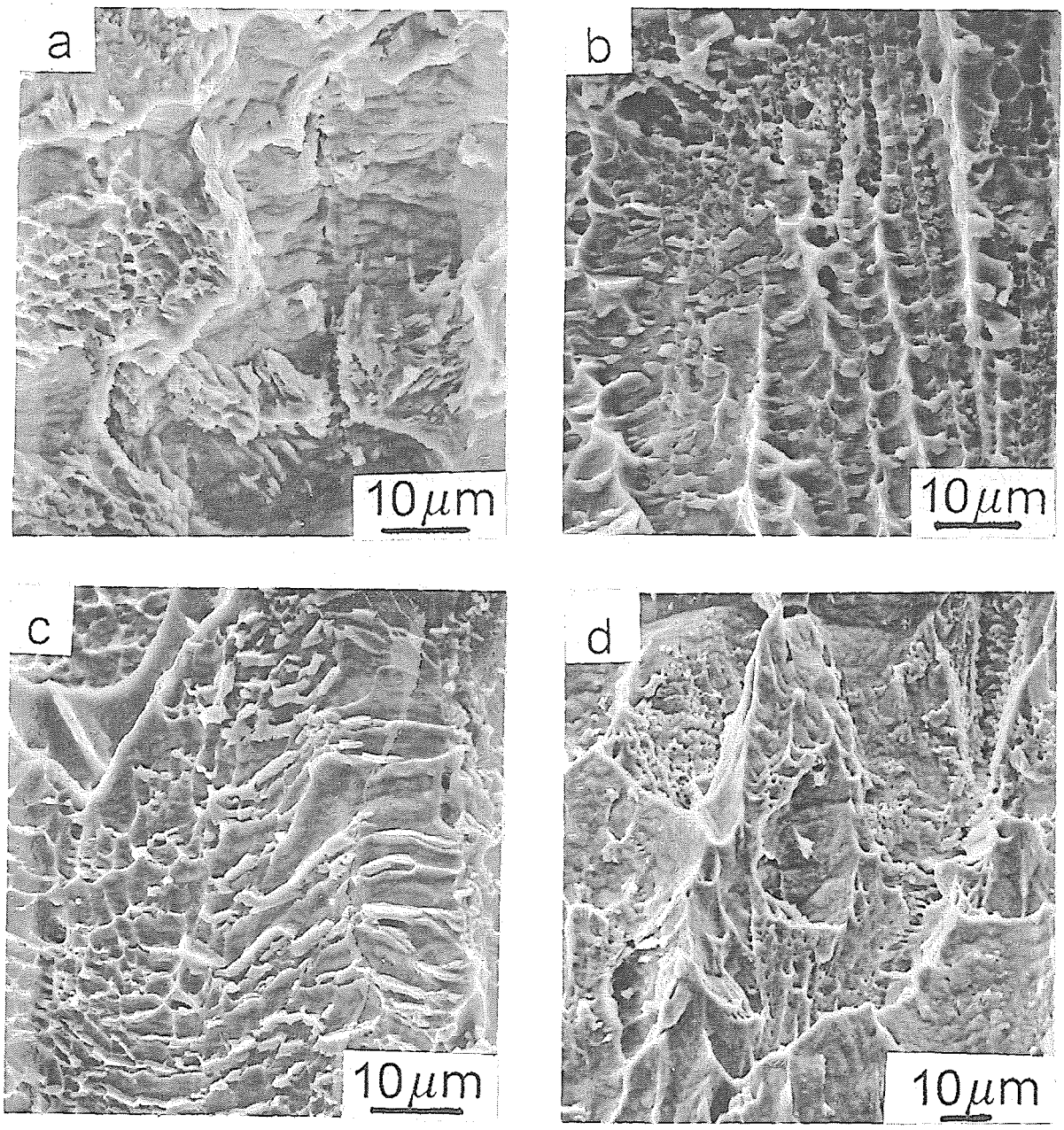

Fig.29: Fracture facets of specimen A2 impact tested at RT (Fig.a), 400 °C (Fig.b), 600 °C (Fig.c) and 800 °C (Fig.d).

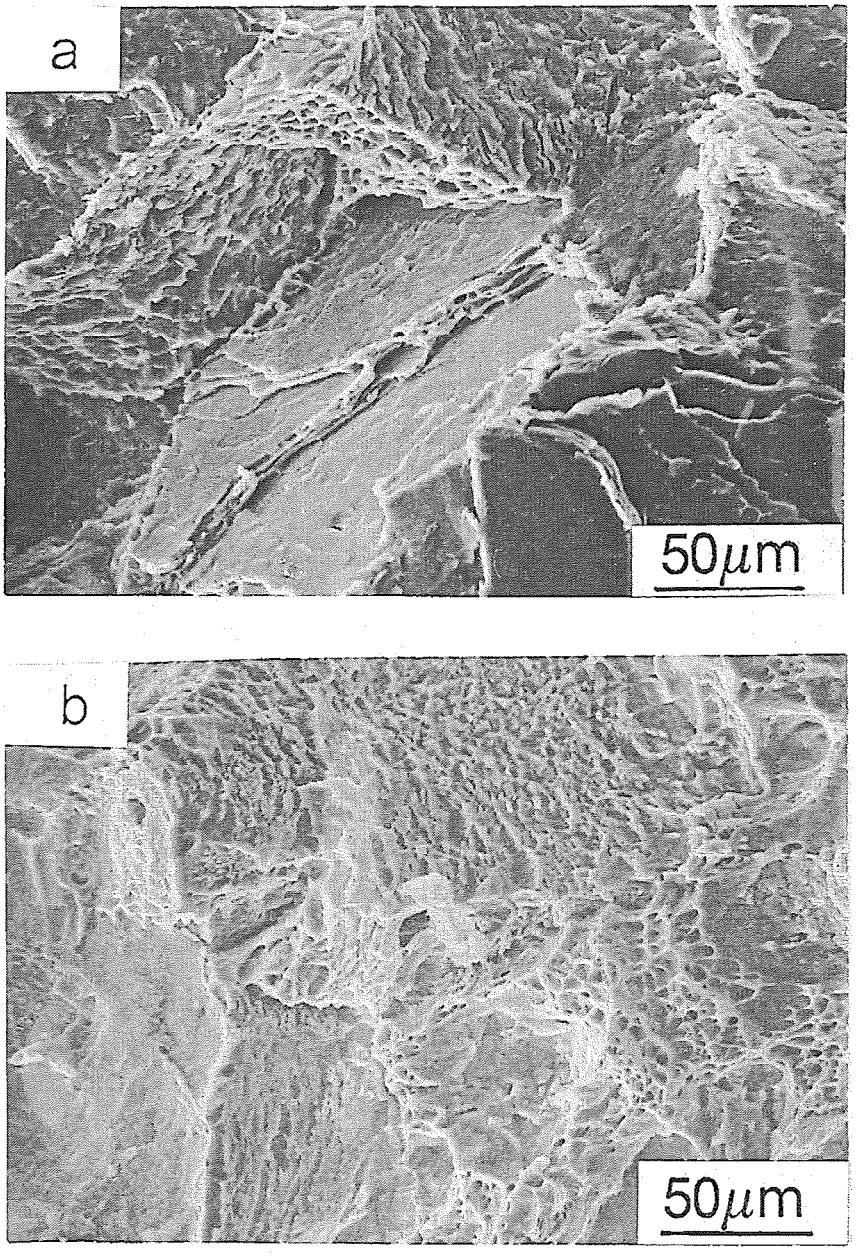

Fig.30: Fracture facets of specimen B2 impact tested at RT: carburized zone (a); non-carburized core (b)

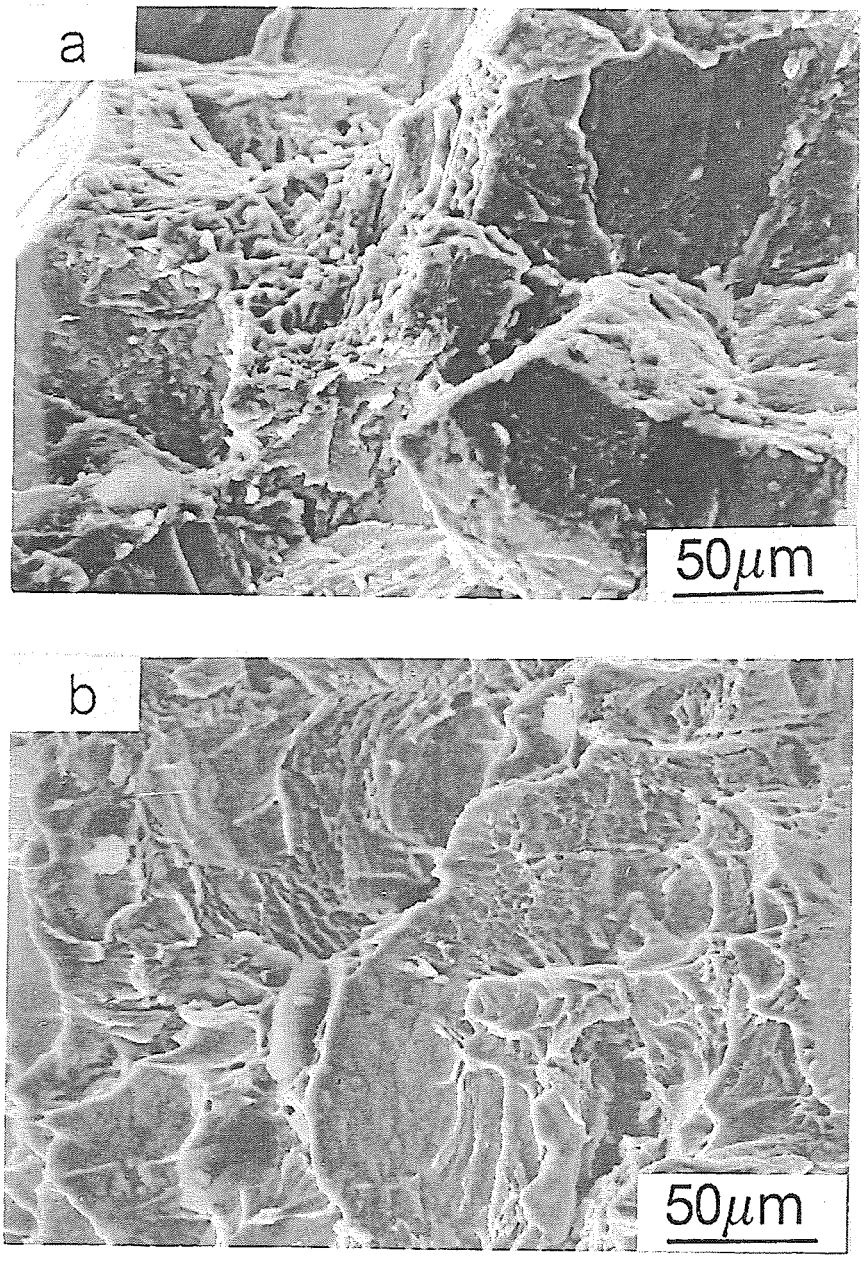

Fig.31: Fracture facets of specimen B2 impact tested at 800 °C: carburized zone (a), non-carburized core (b)

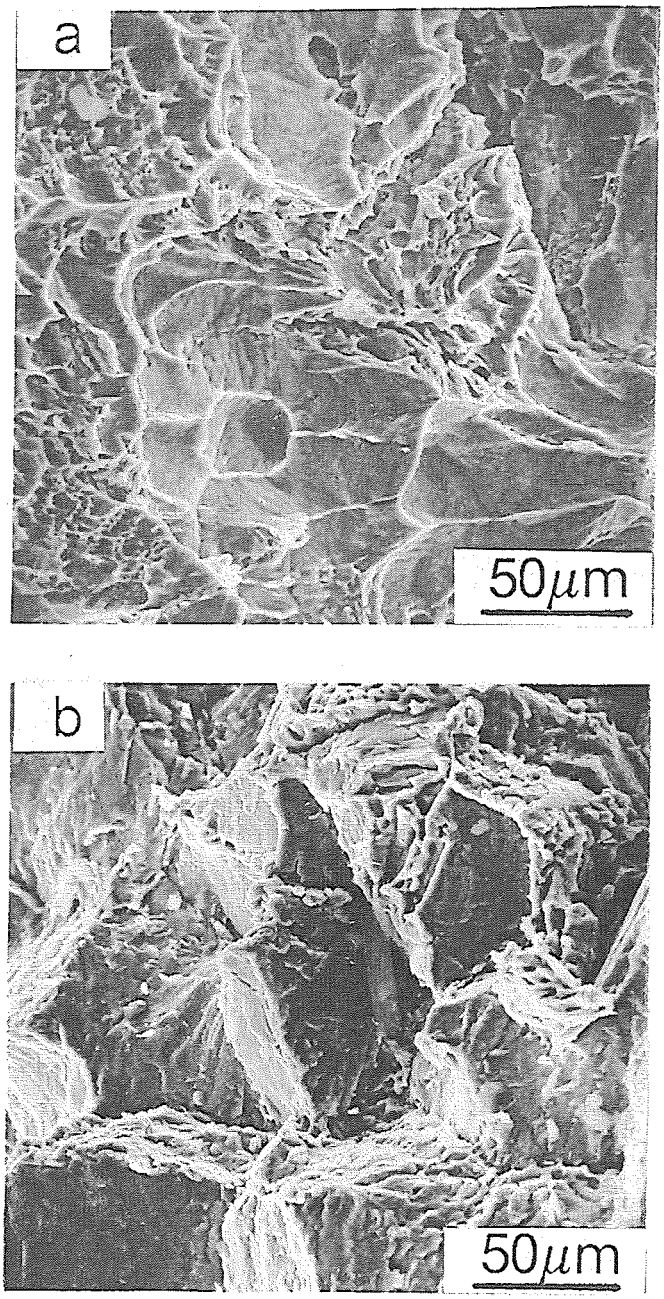

Fig.32: Fracture facets of specimen C tested at 800 °C: carburized zone (a), non-carburized core (b)

FORSCHUNGSZENTRUM JÜLICH GmbH

KFA

Jül-3138
November 1995
ISSN 0944-2952